university of groningen

Industrial Engineering and Management

A pouring application for the Philips Experimental Robotic Arm, using saturated passivity-based control without velocity measurements

Master Thesis

Author:
Floris van den Bos
s2389495

Supervisors:
Prof. Dr. Ir. J.M.A. Scherpen
Dr. L.P. Borja
Dr. M. Muñoz-Arias

August 30, 2019

Abstract

In this thesis, a pouring application is implemented on the Philips Experimental Robotic Arm. For this task only 3 degrees of freedom are considered and set point regulation is used to create the pouring movement. The port-Hamiltonian framework is used to model the system and a passivity-based control approach is adopted to solve the set point regulation problem. The proposed control law is designed to be fully saturated and does not require velocity measurements. Additionally, to eradicate the remaining steady-state error, different integral approaches are implemented and compared. The resulting saturated control is compared against a non-saturated control. Finally, the designed control is combined with force measurements to design a pouring application in which the desired gripper position is controlled based on the measured force caused by the gripped object.

Acknowledgements

First and foremost, I would like to thank my daily supervisor Dr. Pablo Borja. Throughout the writing of this thesis he was always available for questions and willing to make time to help me with my problems. In addition, I would like to thank my first supervisor Prof. Dr. Ir. Jacquelien Scherpen, for her guidance throughout the thesis and for inspiring my interest in the field of control engineering.

Furthermore, I would like to thank my second supervisor Dr. Mauricio Muñoz-Arias, for his knowledge and enthusiasm about the PERA and for making time to help me find solutions to the practical problems.

Finally, I would like to thank Simon Busman and Martin Stokroos, for helping me with all my technical questions, and Sietse Achterop, for his knowledge about the software of the PERA and willingness to help me when errors inevitably occurred.

Contents

Abstract i

Acknowledgements ii

Notation iv

1 Introduction 1
- 1.1 PERA . . . 1
- 1.2 Control of non-linear mechanical systems . . . 2
- 1.3 Problem formulation . . . 3
- 1.4 Outline of the thesis . . . 3

2 Preliminaries 4
- 2.1 Mechanical System Description . . . 4
  - 2.1.1 Denavit-Hartenberg convention . . . 5
  - 2.1.2 Jacobian . . . 6
  - 2.1.3 Inertia matrix . . . 7
  - 2.1.4 Potential energy . . . 7
- 2.2 The Port-Hamiltonian Framework for Mechanical Systems . . . 7
- 2.3 Passivity . . . 9
- 2.4 Stability . . . 10
  - 2.4.1 Lyapunov's Direct Method . . . 11
  - 2.4.2 LaSalle's Invariance Principle . . . 11
  - 2.4.3 Lyapunov's Indirect Method . . . 12
  - 2.4.4 Stability and Passivity . . . 13
- 2.5 Passivity of Port-Hamiltonian Systems . . . 13
- 2.6 Passivity-Based Control . . . 14
  - 2.6.1 PBC of port-Hamiltonian systems . . . 14

3 Philips Experimental Robotic Arm 16
- 3.1 Kinematics . . . 17
- 3.2 Inertia Matrix . . . 19
- 3.3 Potential Energy . . . 19
- 3.4 Current setup . . . 19
- 3.5 Gripper . . . 20
- 3.6 Differential drives . . . 21

3.7 Boards 22
3.8 Motor input and limits 23

4 Control Design **25**
4.1 Passivity-Based Control 25
4.2 Saturated Control 27
4.3 Saturated control without velocity measurements 29
4.4 Gripping control 33

5 Results and Discussion **34**
5.1 Simulation results 35
5.2 Experimental results 36
5.3 Integral term 36
5.4 Non-saturated control 42
5.5 Gripper control 46

6 Conclusion **49**
6.1 Future research 50

Appendices **51**
A PERA Wiring Diagram 52
B Wiring Changes PERA 53

References **54**

Notation

- All vectors are column vectors, unless specified otherwise.
- An $n \times m$ matrix A is denoted by $A_{n\times m}$, an $n \times m$ matrix of zeros is denoted by $0_{n\times m}$ and an $n \times n$ identity matrix is denoted by $I_{n\times n}$.
- For a scalar function $V(x)$ with $x = (x_1, ..., x_n)^\top$, its partial derivative and Hessian are denoted by

$$\frac{\partial V}{\partial x}(x) := \begin{bmatrix} \frac{\partial V}{\partial x_1} \\ \vdots \\ \frac{\partial V}{\partial x_n} \end{bmatrix}, \qquad \frac{\partial^2 V}{\partial x^2}(x) := \begin{bmatrix} \frac{\partial^2 V}{\partial x_1^2} & \cdots & \frac{\partial^2 V}{\partial x_1 \partial x_n} \\ \vdots & \ddots & \vdots \\ \frac{\partial^2 V}{\partial x_n \partial x_1} & \cdots & \frac{\partial^2 V}{\partial x_n^2} \end{bmatrix}.$$

- The use of a subscripted asterisk indicates the desired value of the variable and an asterisk outside a bracket indicates the contents of the brackets are evaluated at the desired value, i.e.

$$V(x)|_* = [V(x)]_* = (V(x))_* = V(x_*).$$

- The range of all non-negative real numbers is denoted by $\mathbb{R}_+$, i.e.

$$\mathbb{R}_+ := [0, \infty).$$

- The Euclidean norm of vector x is denoted by $||x||$.
- e_i denote the unity vectors of the standard basis. In an n-dimensional Euclidean space, the standard basis consists of

$$\begin{aligned} e_1 &= (1, 0, 0, ..., 0, 0)^\top, \\ e_2 &= (0, 1, 0, ..., 0, 0)^\top, \\ &\vdots \\ e_n &= (0, 0, 0, ..., 0, 1)^\top. \end{aligned}$$

- Abuse of notation is often made by leaving out arguments.

Chapter 1

Introduction

The term *robot* was introduced in the 1920 play R.U.R. (*Rossum's Universal Robots*), where it referred to artificial humanoids. Since then, robots have become increasingly important in everyday live, automating industrial processes, operating in hazardous environments or performing precision tasks [6; 7]. A great amount of variety in robotics has been developed. In this thesis, we will focus on one particular robot, the Philips Experimental Robotic Arm (PERA). We aim to carry out a pouring application, by designing a controller for the PERA that takes into account possible implementation issues, such as the saturation of the actuators and the lack of velocity sensors. Towards this end, we adopt a port-Hamiltonian framework to model the robotic arm, and a passivity-based control approach to solve the problem of set point regulation. In this introductory chapter we will first give a brief introduction on the PERA. Next, we will elaborate on control of non-linear mechanical systems such as the PERA, and we will introduce the port-Hamiltonian framework. We will finalize the chapter with a problem formulation and an outline of the rest of the thesis.

1.1 PERA

The PERA is an experimental robotic arm created by Philips Applied Technologies with the intention to be used as a research tool [19]. It is designed after a human arm, with shoulder, elbow and wrist joints, an upper and lower arm, and a gripper with two fingers. It has a total of 7 degrees of freedom (DOF), excluding the movement of the gripper. The fact

that the PERA is equipped with force and position sensors makes a wide variety of research applications possible, with suggested research fields being artificial intelligence, control and dynamics. For the pouring application designed in this thesis, only 3 DOF of the PERA are required, for which we aim to design an appropriate control law. Two limitations arise when working with the PERA, the first of which is the lack of velocity sensors. Because of this, velocity measurements cannot be used in any designed control law. The second limitation is the maximum allowable current of the joint motors. Exceeding the maximum allowable current can cause irreparable damage to an electric motor. Even though fail-safes might be in place in the hardware, exceeding maximum allowable currents is inefficient. Therefore, we aim to design a control law that is saturated, meaning that the input to the system cannot exceed a specified limit. A further description of the PERA is given in Chapter 3.

1.2 Control of non-linear mechanical systems

To design control laws for nonlinear mechanical systems, such as the PERA, a number of tools exist [9; 21; 22]. One of those tools is passivity-based control of port-Hamiltonian systems [23]. The port-Hamiltonian framework has received increasing attention since its introduction in [12]. In comparison to the Euler-Lagrange and Newtonian frameworks, it gives a better representation of the energy in a system, as it is modeled around the Hamiltonian. For mechanical systems, this is the total energy of the system. Additionally, the structure of the port-Hamiltonian framework underscores the interconnection of different parts of the system and shows where energy is dissipated [5]. These concepts, in particular energy, are familiar in many disciplines, including engineering, physics and mathematics. Therefore, the port-Hamiltonian framework provides an intuitive methodology to model complex physical systems and establishes a *lingua franca* among different disciplines.

Another feature of port-Hamiltonian systems is that they are naturally passive, which means that there is no internal energy generation. This feature allows for passivity-based control [23]. More information on the port-Hamiltonian framework and passivity-based control is given in Chapter 2.

At the University of Groningen, the PERA, described in the port-Hamiltonian framework, has been the subject of a number of studies [1; 11; 14; 20]. More recently, passivity-based

control for port-Hamiltonian systems was used to find saturated control laws for set point regulation and pick and place routines for planar, flexible-joint manipulators, without the need for velocity measurements [24; 25]. This thesis will continue on this line of research and apply it to the more complex PERA, where, in contrast to the planar manipulator, gravity compensation is required.

1.3 Problem formulation

The aim of this thesis is to carry out a pouring application on the PERA, where a flexible container can be poured empty, without crushing the container in the progress. This goal is divided into two parts. First, the pouring movement is executed using set point regulation. A control law must be designed that can efficiently perform set point regulation on the PERA with 3 DOF, namely the shoulder yaw joint and the elbow pitch and yaw joints. As mentioned before, due to the limitations of the PERA, we aim to find a control law that does not require velocity measurements and is saturated. Second, after an appropriate control law for set point regulation is designed, we aim to design a control sequence for the gripper. Force measurements are used as feedback to control the gripping behaviour.

1.4 Outline of the thesis

The remainder of this thesis is organized as follows. Chapter 2 provides the theoretical background used in this thesis and in Chapter 3 preliminary information on the PERA is given. Chapter 4 is devoted to the design of the saturated control without velocity measurement and the construction of the gripping control sequence. The designed control law and gripping control sequence are tested and the results are shown and discussed in Chapter 5. Additionally, this chapter gives the addition of an integral term on the control law and compares it to a non-saturated version. Finally, in Chapter 6, a conclusion is given and suggestions for future research are made.

Chapter 2

Preliminaries

In this chapter, an overview of the theoretical background of this thesis is given. The chapter starts with a brief recap on the description of mechanical systems, explaining how systems can be modeled using the Denavit-Hartenberg convention and how the inertia matrix and potential energy can be derived. Then, we give an overview of the port-Hamiltonian framework and, specifically, how this framework can be used to describe mechanical systems. Next, we elaborate on the concepts of passivity and stability, as these concepts play a significant role in the derivation of the control laws of this thesis. Finally, a description of passivity-based control is given.

2.1 Mechanical System Description

The Euler-Lagrange and port-Hamiltonian frameworks provide a systematic way to model mechanical systems. Both approaches require the energy function of the system, which is determined by the potential energy and the so-called inertia matrix. For simple manipulators the identification of the energy function can be straightforward. However, as the number of links increase, this becomes more complex. In this section, methods are described which can be used to derive the inertia matrix and potential energy.

2.1.1 Denavit-Hartenberg convention

A commonly used method to mathematically describe robotic applications is the Denavit-Hartenberg (DH) convention [21]. According to this convention, first the link length a, link twist α, link offset d, and joint angle θ, of each link must be determined. These are usually combined in a so-called DH table. Figure 2.1 shows these parameters of two arbitrary links.

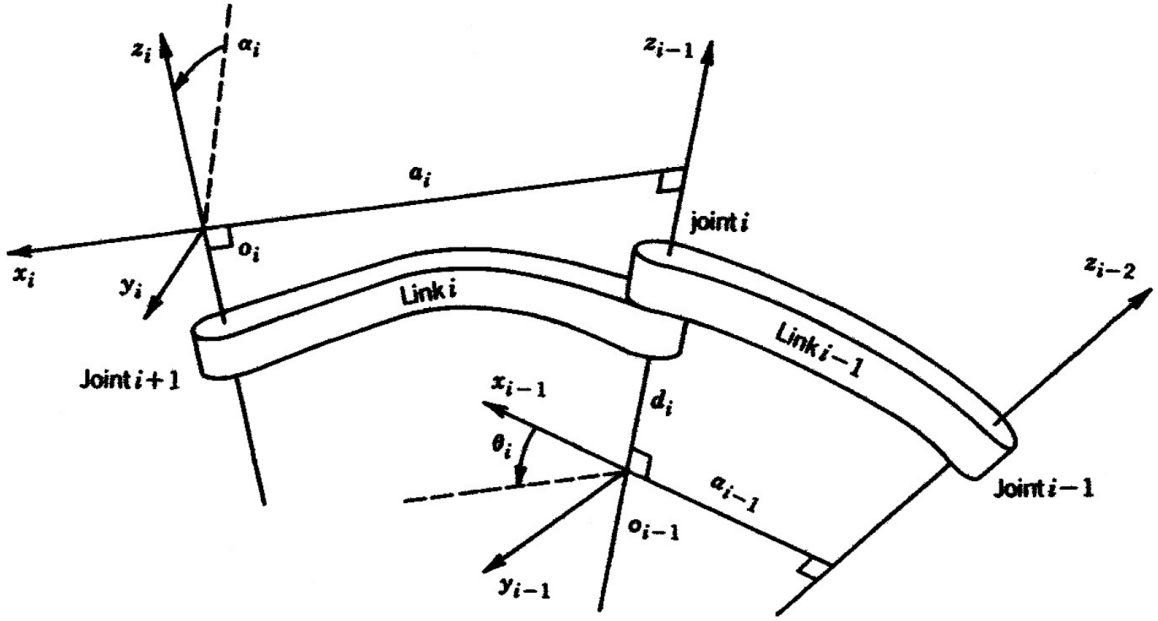

Figure 2.1: Denavit-Hartenberg parameters, from [21]

Using the DH parameters, the transformation matrices can be determined. A homogeneous transformation matrix can be obtained by taking the product of a rotation of α degrees over X, a shift over X by a, a shift over Z by d, and a rotation θ degrees over Z [21]. The resulting homogeneous transformation matrix is given by

$$\begin{aligned} A_i^{i-1} &= Rot_{z,\theta_i} Trans_{z,d_i} Trans_{x,a_i} Rot_{x,\alpha_i} \\ &= \begin{pmatrix} \cos(\theta_i) & -\cos(\alpha_i)\sin(\theta_i) & \sin(\alpha_i)\sin(\theta_i) & a_i\cos(\theta_i) \\ \sin(\theta_i) & \cos(\alpha_i)\cos(\theta_i) & -\sin(\alpha_i)\cos(\theta_i) & a_i\sin(\theta_i) \\ 0 & \sin(\alpha_i) & \cos(\alpha_i) & d_i \\ 0 & 0 & 0 & 1 \end{pmatrix} \end{aligned} \tag{2.1}$$

A transformation matrix from the base frame to the i^{th} link is given by

$$\begin{aligned} \mathcal{T}_i &= A_1^0 A_2^1 ... A_i^{i-1} \\ &= \begin{bmatrix} \mathcal{R}_i & o_i \\ \mathbf{0} & 1 \end{bmatrix}, \end{aligned} \tag{2.2}$$

where $\mathcal{R}_i$ is the 3×3 rotation matrix and o_i is the 3×1 coordinate vector from the base frame to the i^{th} link.

2.1.2 Jacobian

To find the inertia matrix, first the Jacobian of the system must be calculated [21]. The i^{th} column of the Jacobian is given by

$$\mathcal{J}_i = \begin{pmatrix} \mathcal{J}_{v_i} \\ \mathcal{J}_{\omega_i} \end{pmatrix} = \begin{pmatrix} z_{i-1} \times (o_n - o_{i-1}) \\ z_{i-1} \end{pmatrix}, \tag{2.3}$$

where $\mathcal{J}_v$ is the $3 \times n$ linear Jacobian and $\mathcal{J}_w$ is the $3 \times n$ angular Jacobian, and z_{i-1} the third column of rotation matrix $\mathcal{R}_{i-1}$.

For a more realistic description of the system, the center of mass of each link can be taken into account. Equation (2.3) then takes the form

$$\mathcal{J}_i = \begin{pmatrix} \mathcal{J}_{v_i} \\ \mathcal{J}_{\omega_i} \end{pmatrix} = \begin{pmatrix} z_{i-1} \times (o_{c_i} - o_{i-1}) \\ z_{i-1} \end{pmatrix}, \tag{2.4}$$

where o_{c_i} is the vector locating the center of mass of the i^{th} link [21]. To each link corresponds an individual Jacobian. For an n link manipulator, the Jacobians are n columns wide. For the i^{th} link, the first i columns are created using the above mentioned method, the remaining columns consist of zeros.

2.1.3 Inertia matrix

Following [21], the inertia matrix can be calculated by

$$M(q) = \sum_{i=1}^{n} [m_i \mathcal{J}_{v_i}(q)^\top \mathcal{J}_{v_i}(q) + \mathcal{J}_{\omega_i}(q)^\top \mathcal{R}_i(q) \mathcal{I}_i \mathcal{R}_i(q)^\top \mathcal{J}_{\omega_i}(q)], \tag{2.5}$$

where m_i and $\mathcal{I}_i$ are the mass and the inertia tensor of link i, respectively. Note that in equation (2.5) $\mathcal{J}_{v_i}$ and $\mathcal{J}_{\omega_i}$ correspond to the Jacobians of the i^{th} link, not to a column in the Jacobian.

2.1.4 Potential energy

The potential energy of the i$^{\text{th}}$ link is given by :

$$V_i(q) = m_i g^\top o_{c_i} + V_{ref_i} \tag{2.6}$$

where $g^\top$ is the 3×1 gravity vector [21]. V_{ref_i} is a constant chosen so that the minimum value of V_i is zero [3]. As only the partial derivative of the potential energy will be used in the dynamics, V_{ref_i} is arbitrary. The total potential energy is given by the sum of the potential energy of the individual links

$$V(q) = \sum_{i=1}^{n} V_i(q) \tag{2.7}$$

2.2 The Port-Hamiltonian Framework for Mechanical Systems

To express the dynamical behavior of a mechanical system, multiple frameworks exist. One of these frameworks, which is commonly used, is the Euler-Lagrange framework. It can be described by its equation

$$\frac{d}{dt}\left[\frac{\partial L}{\partial \dot{q}}(q, \dot{q})\right] - \frac{\partial L}{\partial q}(q, \dot{q}) = \tau, \tag{2.8}$$

with the Lagrangian function $L(q, \dot{q})$ the difference between the kinetic co-energy and the potential energy, i.e.

$$L(q, \dot{q}) = T^*(q, \dot{q}) - V(q). \tag{2.9}$$

$q = (q_1, q_2, ..., q_n)^\top$ are the generalized coordinates for a system with n degrees of freedom and $\tau \in \mathbb{R}$ are the external forces applied to the system. For mechanical systems, the kinetic

co-energy is often given by

$$T^*(q,\dot{q}) = \frac{1}{2}\dot{q}^\top M(q)\dot{q}, \tag{2.10}$$

where $M(q)$ is the inertia matrix, which is positive and symmetric for all q.

Another method is the port-Hamiltonian framework, described by Maschke and van der Schaft [12]. In this framework the state vector is given in terms of positions and momenta, and the dynamics that describe the behavior of the system are described by the following dynamics [23]

$$\begin{aligned} \dot{q} &= \frac{\partial H}{\partial p}(q,p) \\ \dot{p} &= -\frac{\partial H}{\partial q}(q,p) - D(q,p)\frac{\partial H}{\partial p}(q,p) + u, \end{aligned} \tag{2.11}$$

where $p = (p_1, ..., p_n)^\top$ are the generalized momenta and H is the Hamiltonian, derived from the Lagrangian by performing the Legendre transformation

$$\begin{aligned} H(q,p) &= p^\top \dot{q} - L \\ &= \frac{1}{2}p^\top M^{-1}(q)p + V(q) \\ &= T(q,p) + V(q). \end{aligned} \tag{2.12}$$

As shown in equation (2.12), the Hamiltonian is equal to the total energy in the system. For an n-DOF mechanical system, the system can be described by

$$\begin{aligned} \begin{bmatrix} \dot{q} \\ \dot{p} \end{bmatrix} &= \begin{bmatrix} 0_{n\times n} & I_{n\times n} \\ -I_{n\times n} & -D(q,p) \end{bmatrix} \begin{bmatrix} \frac{\partial H}{\partial q}(q,p) \\ \frac{\partial H}{\partial p}(q,p) \end{bmatrix} + \begin{bmatrix} 0_{nxn} \\ G(q) \end{bmatrix} u \\ y &= G(q)^\top \frac{\partial H}{\partial p}(q,p), \end{aligned} \tag{2.13}$$

where $D(q,p) \in \mathbb{R}_{nxn}$ is the damping matrix and $G(q) \in \mathbb{R}_{nxn}$ is the input matrix. Note that in this thesis natural damping of the PERA is ignored and the system is fully actuated. Therefore, $D(q,p) = 0_{n\times n}$ and $G(q) = I_{n\times n}$. The port-Hamiltonian framework can be generalized as follows to include generalized state variables $x = (x_1, ..., x_{2n})^\top$

$$\begin{aligned} \dot{x} &= [J(x) - R(x)]\frac{\partial H}{\partial q}(x) + g(x)u \\ y &= g(x)^\top \frac{\partial H}{\partial p}(x). \end{aligned} \tag{2.14}$$

Here $x = (x_1, ..., x_{2n})^\top$ are the generalized coordinated, $J(x)$ is the $2n \times 2n$ interconnection matrix and $R(x)$ is the $2n \times 2n$ damping matrix, with

$$\begin{aligned} J(x) &= -J(x)^\top \\ R(x) &= R(x)^\top \geq 0. \end{aligned} \tag{2.15}$$

This generalization is useful to model systems in other domains, e.g. electrical systems, fluid systems or electro-mechanical systems. For more information on the port-Hamiltonian framework, the reader is referred to [23].

2.3 Passivity

Roughly speaking, a system is passive when it cannot generate energy by itself. In passive systems, the rate at which the energy flows into the system is not less than the increase in stored energy. In other words, a passive system cannot store more energy than is supplied to it from the outside, with the difference being the dissipated energy [16]. Passivity has its roots in electrical circuit theory [13]. Passive components, such as inductors and capacitors, can store energy and later release it, but they can never release more energy than they were supplied. The groundwork for passive and dissipative systems was laid by Willems in [26]. Later, his work was extended by Hill and Moylan [8]. Definitions 2.1 and 2.2 formalize these concepts [23].

Consider a system of the form

$$\begin{aligned} \dot{x} &= f(x, u),\ u \in U, \\ y &= h(x, u),\ y \in Y, \end{aligned} \tag{2.16}$$

with states $x = (x_1, ..., x_n)^\top$ and linear spaces U and Y of dimension m. Consider a function

$$s : U \times Y \to \mathbb{R} \tag{2.17}$$

called the *supply rate*.

Definition 2.1. A system (2.16) is said to be *dissipative* with respect to the supply rate $s(t)$ if there exists a function $S : \mathbb{R}^n \to \mathbb{R}_+$, called the *storage function* such that for all $x_0 \in \mathbb{R}^n$,

all $t_1 \geq t_0$, and all input functions u

$$S(x(t_1)) \leq S(x(t_0)) + \int_{t_0}^{t_1} s(y(t), u(t))dt, \tag{2.18}$$

where $x_0 = x(t_0)$ and $x(t_1)$ is the state of (2.16) at time t_1 resulting from initial condition x_0 and input function u.

Equation (2.18) is called the *dissipation inequality*. It expresses that the stored energy $S(x(t_1))$ at some future time t_1 can at most be equal to the stored energy at t_0 plus the total supplied energy during the time interval $[t_0, t_1]$. When there is no dissipation in the system, equation (2.18) holds with equality and the system is considered *conservative* with respect to s.

Definition 2.2. A system (2.16) is said to be *passive* if it is dissipative with respect to the supply rate $s = u^\top y$. It is considered *lossless* if it is conservative with respect to $s = u^\top y$

In the case of passivity, y is the *passive output* of the system. The dissipation inequality for passive systems can be written as the power inequality

$$\dot{S}(x(t)) \leq u^\top y, \tag{2.19}$$

showing that the time derivative of the storage function must be smaller than or equal to the supply rate.

A further elaboration on this subject can be found in [23].

2.4 Stability

The concept of stability roughly speaking means that the states of a system remain in a certain region over time. There exist different definitions of the concept of stability. In this work, we are interested in the stability of equilibrium points, sometimes called stability in the sense of Lyapunov after Russian mathematician Aleksandr Mikhailovich Lyapunov [10]. The following definition formalizes the nature of equilibrium points in terms of stability.

Definition 2.3. An equilibrium point x_* is said to be

- *stable* if, for any $\delta > 0$, there exists $\varepsilon > 0$, such that if $||x_0 - x_*|| < \varepsilon$, then $||x(t, x_0) - x_*|| < \delta$ for all $t \geq 0$

- *asymptotically stable* if it is stable, and if in addition there exists some $\varepsilon > 0$, such that $||x_0 - x_*|| < \varepsilon$ implies that $\lim_{t\to\infty} x(t, x_0) = x_*$
- *globally asymptotically stable* if asymptotic stability holds for any $x_0 \in \mathbb{R}^n$.

2.4.1 Lyapunov's Direct Method

Lyapunov developed two methods to determine the stability of equilibrium points. *Lyapunov's direct method*, uses a generalized energy function $V(x)$, known as the *Lyapunov function* [10].

Consider an equilibrium point x_*. If there is a neighborhood Ω of x_* and a function $V : \Omega \to \mathbb{R}$ such that on Ω

1. $V(x)$ is continuously differentiable,
2. $V(x)$ is positive definite relative to x_*,
3. $\dot{V}(x)$ is negative semi-definite relative to x_*, i.e. $\dot{V}(x) = \sum_{i=1}^{n} \left(\frac{\partial V}{\partial x}\right)^\top \dot{x} \leq 0$

then x_* is a stable equilibrium and $V(x)$ is a Lyapunov function. If additionally $\dot{V}$ is negative definite, then x_* is *locally asymptotically stable.*

If additionally,

4. $V(x)$ is *radially unbounded*, i.e. $V(x) \to \infty$ as $||x|| \to \infty$,

then x_* is *globally asymptotically stable.*

Note here that condition 2 for a multivariable $V(x)$ can be verified if:

1. $\frac{\partial V}{\partial x}(x)|_{x=x_*} = 0_{nx1}$
2. $\frac{\partial^2 V}{\partial x^2}(x)|_{x=x_*} > 0$

2.4.2 LaSalle's Invariance Principle

In practice, it is often hard to prove asymptotic stability using Lyapunov's direct method. This is because $\dot{V}$ does not always depend on all states and is therefore not positive-definite with respect to the equilibrium point. However, in this case *LaSalle's invariance principle* can be used to prove asymptotic stability [10]. To give the principle, we first define an invariant set:

Definition 2.4. A set, $\mathbb{S}$ is an invariant set for a dynamic system if every system trajectory that starts from a point in $\mathbb{S}$ remains in $\mathbb{S}$ for all future time.

Theorem 2.4.1. *Consider an autonomous system* (2.13) *without input, with equilibrium* x_*. *Let* V *be a Lyapunov function on some neighborhood* Ω *of* x_*. *The set* Ω *contains a compact invariant set* $\mathcal{K}$ *in the neighborhood of* x_*. *For every* $x_0 \in \mathcal{K}$ *the solution* $x(t)$ *converges to* $\mathcal{G} := \{x_* \in \mathcal{K} | \dot{V}(x(t; x_*)) = 0 \ \forall t \geq 0\}$ *as* $t \to \infty$.
This subset is invariant and nonempty. If $\mathcal{G} = \{x_*\}$ *then* x_* *is an asymptotically stable equilibrium.*

For a formal proof of this theorem, see [10].

2.4.3 Lyapunov's Indirect Method

Lyapunov's indirect method uses linearization to approximate nonlinear systems as linear systems. By investigating the equilibrium of the linear system, we can draw conclusions about the equilibrium of the nonlinear system. This is formalized in the following theorem [10].

Theorem 2.4.2. *Let* x_* *be an equilibrium for the nonlinear system* $f(x) = x$, *with* $f : D \to \mathbb{R}^n$ *continually differentiable and* D *the neighborhood of* x_*. *Let*

$$A_f = \frac{\partial f}{\partial x}(x)\Big|_{x=x*}, \tag{2.20}$$

then

1. x_* *is an asymptotically stable equilibrium of the nonlinear system if all eigenvalues of* A_f *have a strictly negative real part,*
2. x_* *is an unstable equilibrium of the nonlinear system if one or more of the eigenvalues of* A_f *have a positive real part.*

For a formal proof of this theorem see [10].

2.4.4 Stability and Passivity

An interesting feature of passivity is that it can be used to proof stability. Recall the time derivative of the storage function

$$\dot{S}(x(t)) \leq u^\top y \tag{2.21}$$

Now suppose that the supplied energy is equal to zero. Then, if S is positive definite with respect to x_*, S is a Lyapunov function and the x_* is a stable equilibrium [13].

2.5 Passivity of Port-Hamiltonian Systems

The port-Hamiltonian framework is convenient to show the passivity property of a system, where the Hamiltonian arises as a natural choice for the storage function. Port-Hamiltonian systems are defined by their Hamiltonian function and two geometric structures, $J(q)$ and $R(q)$, corresponding to power conserving interconnection and energy dissipation, which cause the Hamiltonian function to automatically satisfy the dissipation inequality (2.18) [23].

When we take the time derivative of the Hamiltonian

$$\begin{aligned}
\dot{H} &= \left(\frac{\partial H}{\partial q}\right)^\top \dot{q} + \left(\frac{\partial H}{\partial p}\right)^\top \dot{p} \\
&= \left(\frac{\partial H}{\partial q}\right)^\top \frac{\partial H}{\partial p} + \left(\frac{\partial H}{\partial p}\right)^\top \left(-\frac{\partial H}{\partial q} - D\frac{\partial H}{\partial p} + u)\right) \\
&= \left(\frac{\partial H}{\partial q}\right)^\top \frac{\partial H}{\partial p} - \left(\frac{\partial H}{\partial p}\right)^\top \frac{\partial H}{\partial q} - \left(\frac{\partial H}{\partial p}\right)^\top D\frac{\partial H}{\partial p} + \left(\frac{\partial H}{\partial p}\right)^\top u \\
&= -\left(\frac{\partial H}{\partial p}\right)^\top D\frac{\partial H}{\partial p} + y^\top u \leq y^\top u,
\end{aligned} \tag{2.22}$$

we see that it is passive with respect to its passive output $y^\top$, when H is non-negative. When damping is ignored

$$\dot{H} = y^\top u \tag{2.23}$$

and the system is passive and lossless. We can also see that, when H is non-negative, it is a Lyapunov function.

2.6 Passivity-Based Control

Passivity-based control (PBC), first mentioned in [17], is defined as a controller design methodology which achieves stabilization by rendering the system passive with respect to a desired storage function and injecting damping [15; 16; 18].

PBC methods can be classified in two groups: "classical" PBC, where we select the storage function to be assigned a priori, and the second group, where the closed loop storage function is not selected a priori, but is obtained as a result of the desired subsystems interconnections and damping [15; 18]. During this thesis, we focus on classical PBC.

Classical PBC is based around the principle that the point where the open-loop energy is minimal usually is not the one of practical interest. We introduce an input such that the system becomes passive, with a minimum of the storage function at the desired equilibrium x_*. This process is called *energy shaping*. Damping is often injected to ensure asymptotic stability.

2.6.1 PBC of port-Hamiltonian systems

The version of classical PBC used in this thesis is based on the one reported in [2]. In this method, energy shaping of port-Hamiltonian systems is performed where the Hamiltonian acts as a natural storage function. A benefit of this method is that it does not require the solving of partial differential equations.

Consider the generalized system (2.14). We select a control law

$$u = \alpha(x) + v \tag{2.24}$$

such that (2.14) takes the form

$$\begin{aligned} \dot{x} &= [J(x) - R(x)] \frac{\partial H_d}{\partial x}(x) + g(x)v \\ y &= g(x)^\top \frac{\partial H_d}{\partial x}(x). \end{aligned} \tag{2.25}$$

H_d is the desired Hamiltonian, which has a minimum in x_*, that is

$$\frac{\partial H_d}{\partial x}(x)|_* = 0_{nx1} \tag{2.26}$$

$$\frac{\partial^2 H_d}{\partial x^2}(x)|_* > 0. \tag{2.27}$$

The time derivative of this new energy function is

$$\dot{H}_d = -\left(\frac{\partial H_d}{\partial x}(x)\right)^\top R(x)\frac{\partial H_d}{\partial x}(x) + y^\top v. \tag{2.28}$$

Hence, H_d is non-increasing and by finding an appropriate function for v the system can be rendered asymptotically stable.

The fact that H is non-increasing, in addition with the fact that H_d is positive definite with respect to x_* implies that the equilibrium point is stable. To inject damping, we define v of the form

$$v = -Ky, \tag{2.29}$$

where K is a positive definite matrix. Then

$$\dot{H}_d \leq -y^\top Ky. \tag{2.30}$$

Thus, $\dot{H}_d$ is negative definite with respect to $y = 0$. If it can now be proven that

$$y = 0 \implies x = x_*, \tag{2.31}$$

then we can claim (local) asymptotic stability of x_*.

Chapter 3

Philips Experimental Robotic Arm

In this chapter, a description of the Philips Experimental Robotic Arm is given. The kinematics of the full arm are explained, after which we will reduce the model to the 3 DOF setup used in this thesis. Using the Denavit-Hartenberg parameters, the inertia matrix and potential energy are derived. The following section elaborates on the gripper of the PERA. Next, descriptions of the differential drives and boards of the PERA are given. The final section gives information about the motor input and limits.

Figure 3.1: The PERA

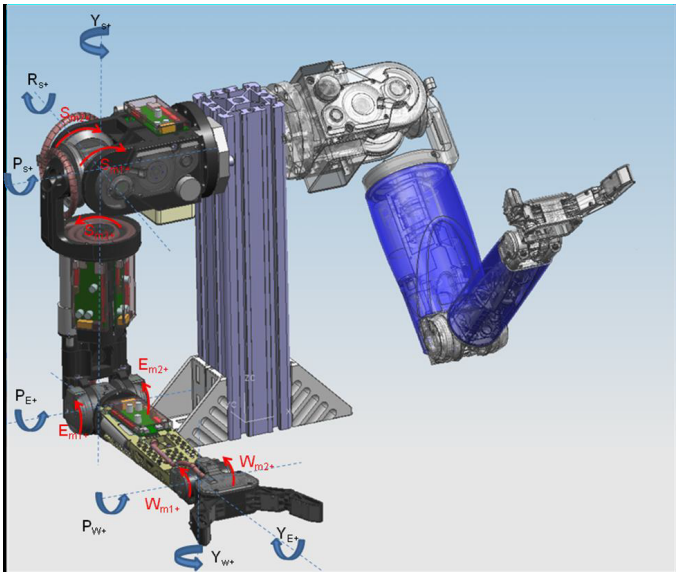

Figure 3.2: Graphical representation of the PERA

3.1 Kinematics

As mentioned before, The PERA, shown in Figure 3.1, is an experimental robotic arm created by Philips Applied Technologies [19]. Figure 3.2 shows a graphical representation of the PERA, including directions of movement of each of the joints. Table 3.1 shows the names for each joint, the corresponding angles and the minimum and maximum for these angles. R, P and Y and the subscripts S, E and W are abbreviations for roll, pitch, yaw, shoulder, elbow and wrist, respectively.

Joint	Angle	Minimum	Maximum
R_S	q_1	$0°$	$+90°$
P_S	q_2	$-90°$	$+90°$
Y_S	q_3	$-90°$	$+90°$
P_E	q_4	$-90°$	$+55°$
Y_E	q_5	$-105°$	$+105°$
P_W	q_6	$-57°$	$+57°$
Y_W	q_7	$-45°$	$+45°$

Table 3.1: Minimum and maximum angles for the PERA, with Figure 3.2 as zero position

The spatial dynamics of the arm have been described in a number of studies [1; 11; 14]. To calculate the inertia matrix and potential energy, we will use the DH representation of [14]. This representation for the 7 DOF arm is given in Figure 3.3. During this thesis, we will only focus on the shoulder yaw joint and the elbow pitch and roll joints, corresponding to q_3, q_4 and q_5 in Figure 3.3.

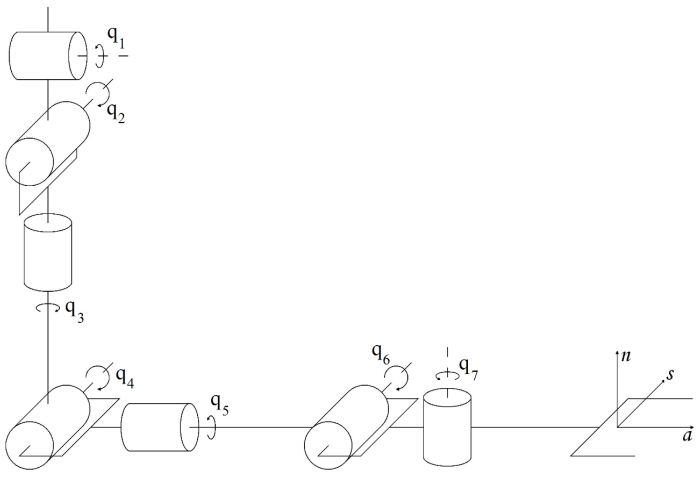

Figure 3.3: Denavit-Hartenberg representation of the PERA [14]

The adjusted DH representation for the 3 DOF arm is given in Figure 3.4. The new notation for the respective joints is q_1 for the shoulder yaw joint, q_2 for the elbow pitch joint and q_3 for the elbow roll joint.

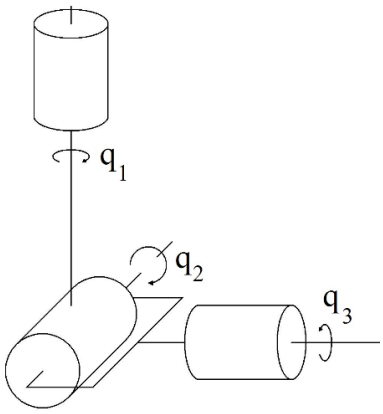

Figure 3.4: Denavit-Hartenberg representation of the PERA with 3 DOF

The DH parameters for this configuration are given in Table 3.2.

link	$\mathbf{a_i}$	$\alpha_\mathbf{i}$	$\mathbf{d_i}$	$\theta_\mathbf{i}$	$\mathbf{a_{ci}}$	$\mathbf{d_{ci}}$
1	0	$\frac{\pi}{2}$	d_1	q_1	0	d_{c1}
2	0	$-\frac{\pi}{2}$	0	$q_2 + \frac{\pi}{2}$	0	0
3	0	0	d_2	q_3	0	d_{c2}

Table 3.2: The Denavit-Hartenberg parameters for the 3 DOF PERA

To check whether the DH parameters are accurate, a model was created using the Robotic Toolbox in Matlab. The result of this is shown in Figure 3.5. From this, it can be concluded that the DH parameters are accurate.

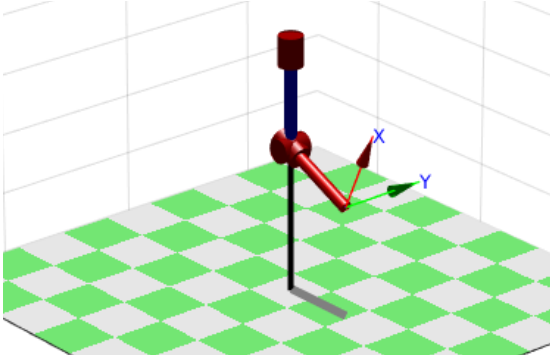

Figure 3.5: Graphical interpretation of the DH table made with the Robotic Toolbox

3.2 Inertia Matrix

Using the parameters from Table 3.2 the transformation matrices and Jacobians are calculated using the methods given in Chapter 2. Using equation (2.5) the Inertia Matrix is

$$M(q) = \begin{bmatrix} \mathcal{I}_1 + \mathcal{I}_2 + \mathcal{I}_3 + m_3 d_{c2}^2 \sin^2(q_2) & 0 & \mathcal{I}_3 \cos(q_2) \\ 0 & \mathcal{I}_2 + \mathcal{I}_3 + m_3 d_{c2}^2 & 0 \\ \mathcal{I}_3 \cos(q_2) & 0 & \mathcal{I}_3 \end{bmatrix}. \tag{3.1}$$

3.3 Potential Energy

Using (2.6) we compute the potential energy, which is given by

$$V(q) = -g d_{c_2} m_3 \cos(q_1) \sin(q_2), \tag{3.2}$$

with its partial derivative

$$\left[\frac{\partial V}{\partial q}(q)\right] = \begin{bmatrix} g d_{c_2} m_3 \sin(q_1) \sin(q_2) \\ -g d_{c_2} m_3 \cos(q_1) \cos(q_2) \\ 0 \end{bmatrix}. \tag{3.3}$$

3.4 Current setup

In the current setup of the hardware, the zero position of the arm is in its downward position. Besides this, the direction of rotation of q_1, q_2 and q_3 are opposite, as in Figure 3.2. Therefore, in the simulations and experiments, equations (3.1)-(3.3) are used with

$$\begin{aligned} q_1 &= -\tilde{q}_1 \\ q_2 &= -\tilde{q}_2 + \frac{\pi}{2} \\ q_3 &= -\tilde{q}_3, \end{aligned} \tag{3.4}$$

where $\tilde{q}_1$, $\tilde{q}_2$ and $\tilde{q}_3$ are the actual angles of the PERA. In the remainder of this thesis, q_1, q_2 and q_3 are used to denote the actual angles of the PERA.

3.5 Gripper

The gripper of the PERA, shown in Figure 3.6, can be considered as the eighth DOF of the PERA [19]. It consists of two fingers which can be opened and closed simultaneously. The gripper is powered by a motor in the lower arm (red rectangle). The rotational movement is converted to a translational movement by a screw (orange rectangle), which is connected to a cable (yellow line), which in turn, is connected to the fingers. When the screw is rotated upward in the arm, the cable pulls the fingers together. When the screw is rotated downward in the arm, the cable pushes the fingers outward. A spring (green line) is located between the two fingers, which exerts a force when the distance between the fingers is less than 4 cm [1]. The gripper, along with the rest of the joints in the PERA, is equipped with a force sensor,

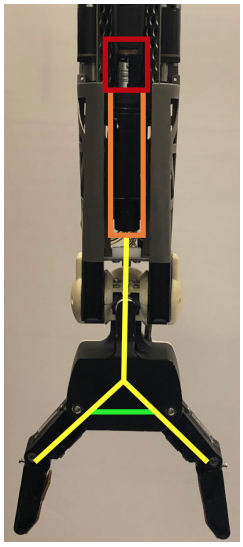

Figure 3.6: The gripper of the PERA

which measures in a dimensionless force. This sensor is placed on the load side of the gearing, such that it is not influenced by the frictional forces of the gears. However, any remaining frictional force, potential force and in the case of the gripper, the force exerted by the spring, are measured along with the external force. For a more elaborate description of these internal forces the reader is referred to [1]. In this thesis the readings of the force sensor are simplified to

$$F_{sensor} = F_{int} + F_{ext}, \tag{3.5}$$

where F_{int} are the combined internal forces and F_{ext} is the normal force exerted by an object on the fingers of the gripper. In [20] the magnitude of the internal force per position of the gripper is measured through experiments. It also shows that the sensor has a range from 0 to 200, after which it is saturated.

In the remainder of this thesis, the position of the gripper will be denoted as q_4. In the current setup, the position is given in radians, with a range of $[0, 0.78]$. The gripper is almost closed at 0 *rad* and fully opened at 0.78 *rad*.

3.6 Differential drives

The PERA is mounted with three differential drives, controlling the shoulder pitch and roll joint, the elbow pitch and yaw joint and the wrist pitch and yaw joints respectively. Only the shoulder yaw joint is controlled by direct rotation. A schematic representation of a differential drive is given in Figure 3.7.

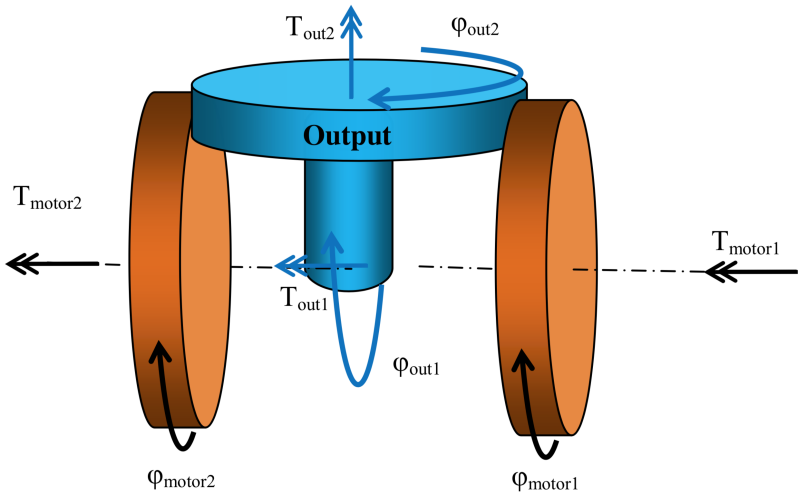

Figure 3.7: Schematic representation of the differential drive used in the PERA [19]

The differential drives consist of two motors connected to two separate gears, G_1 and G_2, which are both connected to a third gear, G_3. When both motors have the same rotational velocity, i.e. $\varphi_{motor1} = \varphi_{motor2}$, G_3 rotates around the axis of G_1 and G_2. When both motors have exactly opposite rotational velocities, i.e. $\varphi_{motor1} = -\varphi_{motor2}$, G_3 rotates around its

own axis. Formally, the outputs of the differential drive are

$$\begin{aligned} \varphi_{out1} &= \frac{1}{2}(\varphi_{motor1} + \varphi_{motor2}) \\ \varphi_{out2} &= \frac{1}{2}(\varphi_{motor1} - \varphi_{motor2}). \end{aligned} \tag{3.6}$$

The relations of the motor torques to the output torques are defined by

$$\begin{aligned} \mathrm{T}_{out1} &= \mathrm{T}_{motor1} + \mathrm{T}_{motor2} \\ \mathrm{T}_{out2} &= \mathrm{T}_{motor1} - \mathrm{T}_{motor2}. \end{aligned} \tag{3.7}$$

During this thesis, only the differential drive of the elbow pitch and yaw joints is considered. In practice, the use of a differential drive means that equations (3.6) and (3.7) must be incorporated in the implementation of a control law. However, it also means that deviations in the movement of the elbow pitch joint can cause deviations in the movement of the elbow roll joint and vice versa.

3.7 Boards

All signals from the sensors to the computer and from the computer to the motors are communicated through boards that are located on the PERA. These boards can be accessed through a USB connection. In total, the PERA is equipped with 4 boards, which are assigned to a set of joints. The original design of the wiring of the PERA is given in Appendix A. Table 3.3 shows which boards correspond to which joints.

Board	Joints
1	R_S, P_S
2	P_E, Y_E
3	Y_S, Gripper
4	P_W, Y_W

Table 3.3: Boards with their corresponding joints

It should be noted that some changes have been made to the wiring of the PERA at the University of Groningen. This is explained in Appendix B.

3.8 Motor input and limits

During this thesis, the proposed control laws u are in the form of torques in $[Nm]$ applied to each DOF. However, the signal that is send to the motors should be the current given in $[mA]$ and the 2 DOFs of the elbow cannot be directly controlled. Therefore, the signal must be converted. First, the differential drive of the elbow needs to be addressed. Equation (3.7) can be rewritten for the input to the motor and in terms of u as

$$\begin{aligned} u_{motor1} &= \frac{1}{2}(u_2 + u_3) \\ u_{motor2} &= \frac{1}{2}(u_2 - u_3). \end{aligned} \tag{3.8}$$

To convert the signals from $[Nm]$ to $[mA]$ the following equation, found in [11] is used

$$u_{PERA} = \frac{u}{Gr * \eta * kM}(1000)(1000)\frac{1}{4.3}. \tag{3.9}$$

Here, u_{PERA} is the input signal send to the PERA and u is either u_1, u_{motor1} or u_{motor2}. Gr is the gear ratio, η is the gear efficiency and kM is the motor torque constant in $[mNm/A]$. These factors are given in Table 3.4. The two factors (1000) are added to convert u to $[mNm]$ and kM to $[mNm/mA]$. The factor $\frac{1}{4.3}$ is added in [11] to compensate for practical issues.

	G	η	kM
Shoulder	66	0.7	53.8
Elbow	33	0.75	23.2
Gripper	66	0.7	25.9

Table 3.4: Motor parameters

To prevent the motors from overheating, a maximum allowable input is given. For the motor of the shoulder yaw joint and both motors of the differential drive of the elbow this is $\pm 16000\ mA$. For the motor of the gripper the maximum allowable input is $\pm 28000\ mA$. The limits can be written in terms of u_1, u_2 and u_3 by combining equations (3.8) and (3.9) and the parameters in Table 3.4:

- $-17.1007 \leq u_1 \leq 17.1007$
- $-7.901 \leq (u_2 + u_3) \leq 7.901$

- $-7.901 \leq (u_2 - u_3) \leq 7.901$

An additional fail-safe is hard-coded into the current setup, limiting the extreme values of u_{PERA} to the specified limits.

Chapter 4

Control Design

In this chapter we design a control law that stabilizes the system, in order to regulate the 3 DOF PERA to a set of desired angles. We propose a passivity-based control law that stabilizes the system, while compensating for the force due to gravity. Then, we modify the control law to make it saturated. Since the PERA does not have velocity sensors, we adjust the saturated control law, such that it does not require velocity measurements. A gripping control sequence is constructed in the final section.

4.1 Passivity-Based Control

To simplify the design, we neglect the natural damping of the system. The behavior of the PERA can then be described by (2.13), with $G = I$, $D = 0$, $y = \dot{q}$ and H given in (2.12).

$$\begin{aligned} \begin{bmatrix} \dot{q} \\ \dot{p} \end{bmatrix} &= \begin{bmatrix} 0_{n\times n} & I_{n\times n} \\ -I_{n\times n} & 0_{n\times n} \end{bmatrix} \begin{bmatrix} \frac{\partial H}{\partial q} \\ \frac{\partial H}{\partial p} \end{bmatrix} + \begin{bmatrix} 0_{n\times n} \\ I_{n\times n} \end{bmatrix} u \\ y &= \frac{\partial H}{\partial p}(q,p) = \dot{q}, \end{aligned} \tag{4.1}$$

where

$$H = \frac{1}{2} p^\top M^{-1}(q) p + V(q). \tag{4.2}$$

Proposition 4.1. *The control law* $u = \frac{\partial V}{\partial q}(q) - ||q - q_*|| - K_p y$ *renders system* (4.1) *asymptotically stable.*

Proof. Following the procedure of [2], we first shape the Hamiltonian such that is has a minimum at the desired equilibrium $(q,p)_* = (q_*, 0_{n\times 1)}$. We introduce a new function $\Phi(q) = V_d(q) - V(q)$, defining the the desired Hamiltonian as

$$H_d(q,p) := H(q,p) + \Phi(q) = \frac{1}{2}p^\top M^{-1}(q)p + V_d(q). \tag{4.3}$$

Following Lyapunov's direct method, the following equations must hold:

$$\begin{bmatrix} \frac{\partial H_d}{\partial q} \\ \frac{\partial H_d}{\partial p} \end{bmatrix}_* = \begin{bmatrix} \frac{\partial V_d}{\partial q}(q) + \frac{1}{2}\sum_{i=1}^{n} e_i p^\top \frac{\partial M_d^{-1}(q)}{\partial q_i} p \\ M_d^{-1}(q)p \end{bmatrix}_* = \begin{bmatrix} \frac{\partial V_d}{\partial q}(q_*) \\ 0_{n\times 1} \end{bmatrix} = \begin{bmatrix} 0_{n\times 1} \\ 0_{n\times 1} \end{bmatrix} \tag{4.4}$$

$$\left[\frac{\partial^2 H_d}{\partial x^2}\right]_* = \begin{bmatrix} \frac{\partial^2 H_d}{\partial q^2} & \frac{\partial^2 H_d}{\partial q \partial p} \\ \frac{\partial^2 H_d}{\partial p \partial q} & \frac{\partial^2 H_d}{\partial p^2} \end{bmatrix}_* = \begin{bmatrix} \frac{\partial^2 V_d}{\partial q^2}|_{q=q_*} & 0_{n\times n} \\ 0_{n\times n} & M^{-1}(q_*) \end{bmatrix} > 0. \tag{4.5}$$

From equations (4.4) and (4.5) it follows that $\frac{\partial V_d}{\partial q}(q_*) = 0_{n\times 1}$ and $\frac{\partial^2 V_d}{\partial q^2}|_{q=q_*} > 0$. Next we evaluate the time derivative of H_d

$$\begin{aligned} \dot{H}_d(q,p) &= \dot{q}^\top u + \Phi(q) = \dot{q}^\top u + \dot{q}\frac{\partial \Phi}{\partial q} = \dot{q}^\top u + \dot{q}^\top \frac{\partial \Phi}{\partial q} \\ &= \dot{q}^\top \left(u + \frac{\partial \Phi}{\partial q}\right). \end{aligned} \tag{4.6}$$

We propose $u = -\frac{\partial \Phi}{\partial \gamma} - K_p\dot{q}$. Where $-K_p\dot{q}$, with $K_p = K_p^\top > 0$, is added to inject damping, changing equation (4.6) to

$$\dot{H}_d(q,p) = -\dot{q}^\top K_p \dot{q} \leq 0. \tag{4.7}$$

Let $\Phi := -V(q) + \frac{1}{2}||q - q_*||^2$, i.e. $V_d(q) = ||q - q_*||^2$. Then

$$\frac{\partial V_d}{\partial q}(q_*) = ||q_* - q_*|| = 0_{n\times 1} \tag{4.8}$$

$$\frac{\partial^2 V_d}{\partial q^2}(q_*) = I_n > 0 \tag{4.9}$$

$$H_d(q,p) = H(q,p) - V(q) + \frac{1}{2}||q - q_*||^2. \tag{4.10}$$

From (4.7) we know that all states converge to the largest invariant set

$$\Omega := \{q, p \in \mathbb{R}^6 | \dot{H}_d = 0_{n\times 1}\}. \tag{4.11}$$

We know that

$$\dot{H}_d = 0_{n\times 1} \Leftrightarrow \dot{q} = 0_{n\times 1} \tag{4.12}$$

$$\dot{q} = M^{-1}(q)p = 0_{n\times 1} \Leftrightarrow p = 0_{n\times 1} \Leftrightarrow \dot{p} = 0_{n\times 1} \tag{4.13}$$

$$\dot{p} = p^\top \frac{\partial M^{-1}}{\partial q} p \Big|_{p=0} + q - q_* = q - q_* = 0_{n\times 1} \Leftrightarrow q = q_*. \tag{4.14}$$

We can conclude that the only invariant set in Ω is $(q,p) = (q_*, 0_{n\times 1})$ and by LaSalle's invariance principle, we can conclude that this equilibrium is asymptotically stable, completing the proof.

4.2 Saturated Control

We would like to adjust the control law such that it becomes saturated. Following [25], we need to replace the terms in the control law with saturated functions. Therefore, we modify the function Φ. Note that we assume the partial derivatives of the potential energy to be saturated. This is the case for the PERA, as can be seen in Equation (3.3), and for many mechanical systems with only gravitational potential energy. However, care should be taken with this assumption, as it does not hold for all mechanical systems, e.g. systems with a linear spring. We again consider the system as (4.1) with Hamiltonian (4.2). The saturated control law is introduced in the following proposition.

Proposition 4.2. *The control law* $u = \frac{\partial V}{\partial q} - \sum_{i=1}^{n} e_i[\alpha_i \tanh(\beta_i \gamma_i) + \alpha_{p_i} \tanh(\beta_{p_i} \dot{q}_i)]$ *renders system* (4.1) *asymptotically stable.*

Proof We define $\gamma := q - q_*$ and $\Phi(\gamma) := V_d(\gamma) - V(q)$. Therefore, the desired Hamiltonian takes the form:

$$H_d(q,p) = H(q,p) + \Phi(\gamma) = \frac{1}{2} p^\top M^{-1}(q) p + V_d(\gamma), \tag{4.15}$$

with V_d a to be designed saturated function. Similar to equations (4.8) and (4.9), the following equations must hold

$$\left(\frac{\partial V_d}{\partial \gamma}\right)_* = 0_{n\times 1} \tag{4.16}$$

$$\left(\frac{\partial^2 V_d}{\partial \gamma^2}\right)_* > 0. \tag{4.17}$$

To satisfy these equations we define

$$V_d(\gamma) = \sum_{i=1}^{n} \frac{\alpha_i}{\beta_i} ln(\cosh(\beta_i \gamma_i)). \tag{4.18}$$

Then

$$\left(\frac{\partial V_d}{\partial \gamma}(\gamma)\right)_* = \left(\sum_{i=1}^{n} e_i \alpha_i \tanh(\beta_i \gamma_i)\right)_* = 0_{n\times 1} \tag{4.19}$$

$$\left(\frac{\partial^2 V_d}{\partial \gamma^2}(\gamma)\right)_* = \left(\sum_{i=1}^{n} e_i e_i^\top \alpha_i \beta_i \operatorname{sech}(\beta_i \gamma_i)\right)_* = diag\{\alpha_1\beta_1, ..., \alpha_n\beta_n\} > 0. \tag{4.20}$$

The time derivative of the desired Hamiltonian becomes

$$\dot{H}_d(q,p) = \dot{q}^\top u + \dot{\Phi} = \dot{q}^\top u + \dot{\gamma}^\top \frac{\partial \Phi}{\partial \gamma} = \dot{q}^\top (u + \frac{\partial \Phi}{\partial \gamma}). \tag{4.21}$$

When

$$\begin{aligned} u :&= -\frac{\partial \Phi}{\partial \gamma} - \sum_{i=1}^{n} e_i \alpha_{p_i} \tanh(\beta_{p_i} \dot{q}_i) \\ &= \frac{\partial V}{\partial q} - \sum_{i=1}^{n} e_i [\alpha_i \tanh(\beta_i \gamma_i) + \alpha_{p_i} \tanh(\beta_{p_i} \dot{q}_i)], \end{aligned} \tag{4.22}$$

$$\dot{H}_d(q,p) = -\sum_{i=1}^{n} \dot{q}_i \alpha_{p_i} \tanh(\beta_{p_i} \dot{q}_i) \leq 0, \ \forall \alpha_i \beta_i > 0, \ i = 1, ..., n. \tag{4.23}$$

We see that all states converge to the invariant set

$$\Omega := \{q, p \in \mathbb{R}^6 | \dot{H}_d = 0_{n\times 1}\}, \tag{4.24}$$

and, similar to (4.12)-(4.14) we have

$$\dot{H}_d = 0_{n\times 1} \Leftrightarrow \dot{q} = 0_{n\times 1} \tag{4.25}$$

$$\dot{q} = M^{-1}(q)p = 0_{n\times 1} \Leftrightarrow p = 0_{n\times 1} \Leftrightarrow \dot{p} = 0_{n\times 1} \tag{4.26}$$

$$\dot{p} = p^\top \frac{\partial M^{-1}}{\partial q} p \Big|_{p=0_{n\times 1}} + q - q_* = q - q_* = 0_{n\times 1} \Leftrightarrow q = q_*. \tag{4.27}$$

We can conclude that the only invariant set in Ω is $(q, p) = (q_*, 0_{n\times 1})$ and by LaSalle's invariance principle, we can conclude that this equilibrium is asymptotically stable. With this, we complete the proof.

Equation (4.22) can be rewritten for each degree of freedom as

$$u_i := \frac{\partial V}{\partial q_i} - \alpha_i \tanh(\beta_i \gamma_i) - \alpha_{p_i} \tanh(\beta_{p_i} \dot{q}_i),\ i = 1, ..., n. \tag{4.28}$$

Due to the special form of the hyperbolic tangent, the second and third term of (4.28) never exceed the range $[-\alpha_i, \alpha_i]$ and $[-\alpha_{p_i}, \alpha_{p_i}]$, respectively. Now, assuming that $\lambda_i \leq \frac{\partial V}{\partial q_i} \leq \rho_i$, with λ_i and ρ_i constants, u_i is saturated with

$$\lambda_i - \alpha_i - \alpha_{p_i} \leq u_i \leq \rho_i + \alpha_i + \alpha_{p_i}. \tag{4.29}$$

With this, we have successfully modified the control law to make it saturated.

4.3 Saturated control without velocity measurements

In the previous control laws, we have injected damping using the passive output of the system, i.e. the velocity. However, velocity measurements are not always available. This is also the case for the PERA, as it does not have velocity sensors. Therefore, we would like to find a control law that does not require velocity measurements. To this end, we again modify the function Φ. A method for injecting damping with only position measurements was proposed in [4]. The control law introduced in the following proposition is based on a variant of this method as proposed in [25].

Proposition 4.3. *The control law* $u = \frac{\partial V}{\partial q} - \sum_{i=1}^{n} e_i \alpha_i \tanh(\beta_i z_i)$*, with* $\alpha_i \beta_i > 0$*, for* $i = 1, ..., n$*, renders system* (4.1) *asymptotically stable.*

Proof. We introduce a new state $x_c \in \mathbb{R}^n$ to system (4.1), such that the $\xi = (q^\top, p^\top, x_c^\top)^\top$ and we can define the system as

$$\begin{bmatrix} \dot{q} \\ \dot{p} \\ \dot{x}_c \end{bmatrix} = \begin{bmatrix} 0_{n\times n} & I_{n\times n} & 0_{n\times n} \\ -I_{n\times n} & 0_{n\times n} & 0_{n\times n} \\ 0_{n\times n} & 0_{n\times n} & -R_c \end{bmatrix} \begin{bmatrix} \frac{\partial H}{\partial q} \\ \frac{\partial H}{\partial p} \\ \frac{\partial H}{\partial x_c} \end{bmatrix} + \begin{bmatrix} 0_{n\times n} \\ I_{n\times n} \\ 0_{n\times n} \end{bmatrix} u, \tag{4.30}$$

with $R_c = R_c^\top > 0$. We define

$$\begin{aligned} \tilde{q} &:= q - q_* \\ z &:= \tilde{q} + x_c \end{aligned} \tag{4.31}$$

and set the desired states $\xi_* = (q^\top, p^\top, x_c^\top)_*^\top = (q_*^\top, 0_{1\times n}, 0_{1\times n})^\top$. When we define $u := \frac{\partial V}{\partial q} + u_{pbc}$ we can define the desired Hamiltonian as

$$H_d(\xi) = T(q,p) + \Phi(z) + \frac{1}{2} x_c^\top K_c x_c, \; K_c > 0 \in \mathbb{R}^{n\times n}. \tag{4.32}$$

Since

$$\frac{\partial z}{\partial q} = \frac{\partial z}{\partial x_c} = I_{n\times n} \tag{4.33}$$

and

$$\frac{\partial \Phi}{\partial z} = \frac{\partial \Phi}{\partial q} = \frac{\partial \Phi}{\partial x_c} \tag{4.34}$$

we find

$$\left(\frac{\partial H_d}{\partial \xi}\right)_* = \begin{bmatrix} \frac{\partial T}{\partial q} + \frac{\partial \Phi}{\partial q} \\ \frac{\partial T}{\partial p} \\ \frac{\partial \Phi}{\partial x_c} + K_c x_c \end{bmatrix}_* = \begin{bmatrix} \frac{\partial \Phi}{\partial z} \\ 0_{n\times 1} \\ \frac{\partial \Phi}{\partial z} \end{bmatrix}_* \tag{4.35}$$

$$\left(\frac{\partial^2 H_d}{\partial \xi^2}\right)_* = \begin{bmatrix} \frac{\partial^2 \Phi}{\partial q^2} & 0_{n\times n} & \frac{\partial^2 \Phi}{\partial q^2} \\ 0_{n\times n} & M^{-1}(q) & 0_{n\times n} \\ \frac{\partial^2 \Phi}{\partial q^2} & 0_{n\times n} & \frac{\partial^2 \Phi}{\partial q^2} + K_c \end{bmatrix}_*. \tag{4.36}$$

To satisfy Lyapunov's direct method we introduce

$$\Phi(z) = \sum_{i=1}^{3} \frac{a_i}{\beta_i} ln(\cosh(\beta_i z_i)),\ \alpha_i\beta_i > 0,\ i = 1, ..., n. \tag{4.37}$$

Then

$$\left(\frac{\partial H_d}{\partial \xi}\right)_* = \begin{bmatrix} 0_{n\times 1} \\ 0_{n\times 1} \\ 0_{n\times 1} \end{bmatrix}_* \tag{4.38}$$

$$\left(\frac{\partial^2 \Phi}{\partial q^2}\right)_* = \begin{bmatrix} \alpha_1\beta_1 & 0 & 0 \\ 0 & \alpha_2\beta_2 & 0 \\ 0 & 0 & \alpha_3\beta_3 \end{bmatrix}_* \tag{4.39}$$

$$\left(\frac{\partial^2 H_d}{\partial \xi^2}\right)_* > 0 \tag{4.40}$$

$$\begin{aligned} \dot{H}_d &= \dot{q}^\top u_{pbc} + \dot{z}^\top \frac{\partial \Phi}{\partial z} + \dot{x}^\top K_c x_c = \dot{q}^\top u_{pbc} + (\dot{q} + \dot{x}_c)^\top \frac{\partial \Phi}{\partial z} + \dot{x}^\top K_c x_c \\ &= \dot{q}^\top (u_{pbc} + \frac{\partial \Phi}{\partial z}) + \dot{x}^\top (K_c x_c + \frac{\partial \Phi}{\partial z}) \\ &= \dot{q}^\top (u_{pbc} + \frac{\partial \Phi}{\partial z}) - (K_c x_c + \frac{\partial \Phi}{\partial z})^\top R_c (K_c x_c + \frac{\partial \Phi}{\partial z}). \end{aligned} \tag{4.41}$$

We define $u_{pbc} := -\frac{\partial \Phi}{\partial z}$, then

$$\dot{H}_d = -(K_c x_c + \frac{\partial \Phi}{\partial z})^\top R_c (K_c x_c + \frac{\partial \Phi}{\partial z}) \leq 0 \tag{4.42}$$

and the input becomes

$$\begin{aligned} u &= \frac{\partial V}{\partial q} - \frac{\partial \Phi}{\partial z} \\ &= \frac{\partial V}{\partial q} - \sum_{i=1}^{n} e_i \alpha_i \tanh(\beta_i z_i). \end{aligned} \tag{4.43}$$

We can conclude that the states converge to the following set

$$\Omega := \{\xi \in \mathbb{R}^9 \mid \dot{H}_d = 0_{n\times 1}\}. \tag{4.44}$$

From (4.42) we know that

$$\dot{H}_d = 0_{n\times 1} \Leftrightarrow K_c x_c + \frac{\partial \Phi}{\partial z} = 0_{n\times 1} \Leftrightarrow \dot{x}_c = 0_{n\times 1} \tag{4.45}$$

$$\frac{d}{dt}\left(K_c x_c + \frac{\partial \Phi}{\partial z}\right) = \frac{\partial^2 \Phi}{\partial z^2}\dot{z} + K_c \cancelto{0_{n\times 1}}{\dot{x}_c} = \underbrace{\frac{\partial^2 \Phi}{\partial z^2}}_{>0}\dot{z} = 0_{n\times 1} \Leftrightarrow \dot{z} = 0_{n\times 1} \tag{4.46}$$

$$\dot{z} = \dot{q} + \cancelto{0_{n\times 1}}{\dot{x}_c} = \dot{q} = 0_{n\times 1} \tag{4.47}$$

$$\dot{q} = M^{-1}(q)p = 0_{n\times 1} \Leftrightarrow p = 0_{n\times 1} \Leftrightarrow \dot{p} = 0_{n\times 1} \tag{4.48}$$

$$\begin{aligned} \dot{p} &= -\frac{\partial H}{\partial q} + u = -\frac{\partial V}{\partial q} - p^\top \cancelto{0_{n\times 1}}{\frac{\partial M^{-1}}{\partial q}} p + \frac{\partial V}{\partial q} - \frac{\partial \Phi}{\partial q} \\ &= -\frac{\partial \Phi}{\partial z} = 0_{n\times 1} \Leftrightarrow z = 0_{n\times 1}. \end{aligned} \tag{4.49}$$

We replace (4.49) in (4.45) and find

$$\dot{x} = -R_c(\underbrace{K_c}_{>0} x_c + \cancelto{0_{n\times 1}}{\frac{\partial \Phi}{\partial z}}) = 0_{n\times 1} \Leftrightarrow x_c = 0_{n\times 1} \tag{4.50}$$

$$z = \tilde{q} + \cancelto{0_{n\times 1}}{x_c} = 0_{n\times 1} \Leftrightarrow \tilde{q} = q - q_* = 0_{n\times 1} \Leftrightarrow q = q_*. \tag{4.51}$$

We find that the states converge to $\xi = (q_*^\top, 0_{1\times n}, 0_{1\times n})^\top$ and, by LaSalle's invariance principle, we can conclude that the system is asymptotically stable, ending the proof.

Similar to the previous section (4.43) can be rewritten for each degree of freedom as

$$u_i = \frac{\partial V}{\partial q_i} - \alpha_i \tanh(\beta_i z_i),\ i = 1, ..., n \tag{4.52}$$

and we can conclude that the input is saturated with

$$\lambda_i - \alpha_i \leq u_i \leq \rho_i + \alpha_i. \tag{4.53}$$

We now have a saturated control law that ensures asymptotic stability of the desired equilibrium and does not require velocity measurements.

4.4 Gripping control

In this section, a heuristic gripping strategy is introduced. The aim of this strategy is to control the gripping force during a pouring exercise, such that the gripping force is reduced when the normal force of the pouring vessel is reduced. An example is a flexible plastic cup filled with a substance that is poured out. During the pouring, the outward pressure of the substance disappears. If the gripper maintains the same force, the plastic cup might be crushed.

First, we define $f(k)$ to be the measured force at time k and to compensate for any noise in the measurements, a moving-average filter is implemented over the force measurements, with

$$f_{MA}(k) = \frac{f(k-m+1) + ... + f(k)}{m}. \tag{4.54}$$

Next, let $\mathcal{F}_{MA} = \{f_{MA}(k-m-1), ..., f_{MA}(k)\}$ be the set of the previous m moving-average forces, with m a positive, even number. Define

$$\begin{aligned} f_a &:= \{f_{MA}(k-m-1), ..., f_{MA}(k-\frac{m}{2}-1)\} \\ f_b &:= \{f_{MA}(k-\frac{m}{2}), ..., f_{MA}(k)\}, \end{aligned} \tag{4.55}$$

such that $\mathcal{F}_{MA} = \{f_a, f_b\}$. The averages values of f_a and f_b are given by $\bar{f}_a$ and $\bar{f}_b$, respectively.

It is assumed that the gripping force is related to the error in the desired position, i.e. to grasp a cup, the desired position is set to a slightly smaller position than the exterior of the cup. Then the following sequence can be used to reduce the gripping force when the normal force is reduced

$$\bar{f}_a - \bar{f}_b = \begin{cases} < l, & q_* = q_* \\ \geq l, & q_* = q \end{cases} \tag{4.56}$$

where l is a certain limit that depends on the specifications of the system. In words, this means that if the average force over a certain time period is significantly lower than the average force before that time period, the desired angle of the gripper is set to the current angle, thereby preventing the gripper from crushing the pouring vessel.

Chapter 5

Results and Discussion

In this chapter, we show the results of a simulation of the control law proposed in proposition 4.3. After this, we show the results of this control law tested on the PERA. Due to a steady-state error found in the experiments, we introduce an integral term on the position. The saturated control law including integral term are compared against a non-saturated control law. In all of these simulations and experiments, the initial angles are set at $(q_1, q_2, q_3) = (-\pi/2, 0, 0)$ and the desired angles at $(q_1, q_2, q_3)_* = (0, \pi/2, 1.7)$, as shown in Figures 5.1 and 5.2. Next, the control law is implemented on the gripper and the gripper control sequence, constructed in section 4.4, is tested in a pouring experiment. The result of this is shown in the final section.

Figure 5.1: Start position

Figure 5.2: Desired position

5.1 Simulation results

A model of the PERA is constructed in Matlab with inertia matrix (3.1) and partial derivative of the potential energy (3.3). Using Simulink, a closed-loop simulation is created with control law $u = \frac{\partial V}{\partial q} - \alpha \tanh(\beta z)$, designed in section 4.3. The parameters are chosen such that the control law remains within the limits of the PERA, as mentioned in section 3.8. With $g = 9.81$, $m_3 = 1$ and $d_{c_2} = 0.1$, the extreme values for the partial derivatives for the potential energy are $max\left(\frac{\partial V}{\partial q}\right) = (\pm 0.981, \mp 0.981, 0)^\top$. We select

$$\begin{aligned} \alpha &= (15, 1.9, 5)^\top \\ \beta &= (30, 40, 30)^\top \\ K_c &= diag\{0.01, 0.01, 0.01\} \\ R_c &= diag\{0.6, 1.1, 0.9\}. \end{aligned} \tag{5.1}$$

With these values for α, the saturation limits are satisfied. Figure 5.3 shows the result of the simulation.

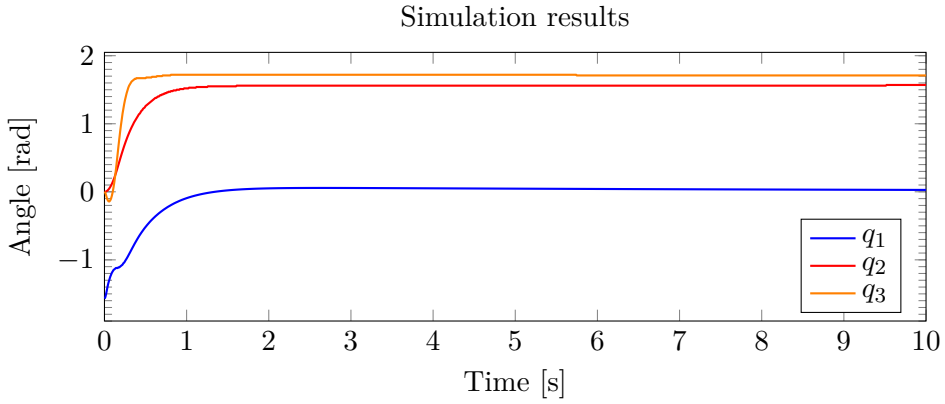

Figure 5.3: Simulation results of the saturated control without velocity measurements

The blue line represents the angle of the shoulder yaw joint, q_1, the red line represents the angle of the elbow pitch joint, q_2, and the yellow line represents the angle of the elbow yaw joint, q_3. We can conclude that the control law performs well, as the angles converge to the desired angles within 2 seconds and no overshoot occurs.

5.2 Experimental results

Next, the control law is tested on the PERA. We select

$$\begin{aligned} \alpha &= (12, 3, 3)^\top \\ \beta &= (80, 40, 40)^\top \\ K_c &= diag\{0.2, 0.2, 0.2\} \\ R_c &= diag\{0.001, 0.001, 0.001\}, \end{aligned} \tag{5.2}$$

satisfying the saturation limits. The experimental result of the control law tested on the PERA are shown in Figure 5.4.

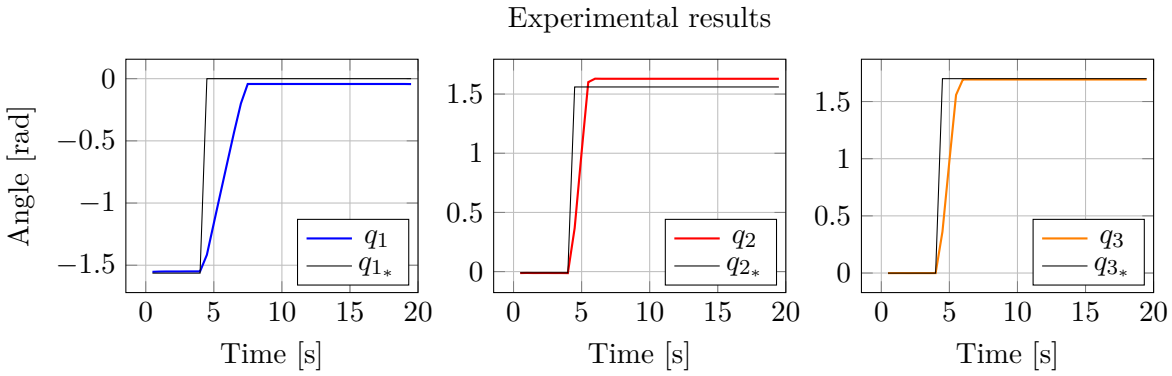

Figure 5.4: Experiment results of the saturated control without velocity measurements

Figure 5.4 shows that the angles quickly approach towards the desired position and there is little overshoot. However, a small steady-state error exists. This error can be caused by internal frictions or natural damping of the system, which are not modeled in the simulation. Another explanation can be that the modeled potential energy is not completely the same as the actual potential energy. In the following section, we address this steady-state error.

5.3 Integral term

In order to compensate for the steady-state error, we introduce an integral term on the position. We consider the system as in (4.30). We define the new state σ, such that $\dot{\sigma}$ is a function of $\tilde{q} = q - q_*$. Next, we introduce the control law $u = \frac{\partial V}{\partial q} - \frac{\partial \Phi}{\partial z} - \frac{\partial \Psi}{\partial \sigma}$. The closed-loop system becomes

$$\left[\dot{\zeta}\right] = \begin{bmatrix} \dot{q} \\ \dot{p} \\ \dot{x}_c \\ \dot{\sigma} \end{bmatrix} = \begin{bmatrix} M^{-1}p \\ -\frac{\partial \Phi}{\partial z} - \frac{\partial \Psi}{\partial \sigma} - \frac{\partial T}{\partial q} \\ -R_c(K_c x_c + \frac{\partial \Phi}{\partial z}) \\ \dot{\sigma}(\tilde{q}) \end{bmatrix} = f(\zeta). \tag{5.3}$$

Note that by adding the integral term, the port-Hamiltonian structure of the closed-loop system is no longer preserved. This means that stability can no longer be proven in the manner done in the previous chapter. Therefore, in the remainder of this chapter, we verify stability using Lyapunov's indirect method. If we define $\Psi = \sum_{i=1}^{3} \frac{\alpha_{\sigma_i}}{\beta_{\sigma_i}} ln(\cosh(\beta_{\sigma_i}\sigma_i))$, the control law remains saturated with

$$\lambda_i - \alpha_i - \alpha_{\sigma_i} \leq u_i \leq \rho_i + \alpha_i + \alpha_{\sigma_i}. \tag{5.4}$$

In order to design an appropriate control law, we try four different dynamics for σ. First, we introduce a simple integral term on the position. Let

$$\dot{\sigma} = \tilde{q}. \tag{5.5}$$

Then, we can linearize the system with

$$A_f = \frac{\partial f}{\partial \zeta}\Big|_{\zeta_*} = \begin{bmatrix} 0_{3\times3} & M^{-1} & 0_{3\times3} & 0_{3\times3} \\ -D_c & 0_{3\times3} & -D_c & -D_\sigma \\ -R_c D_c & 0_{3\times3} & -R_c K_c - R_c D_c & 0_{3\times3} \\ I_{3\times3} & 0_{3\times3} & 0_{3\times3} & 0_{3\times3} \end{bmatrix}, \tag{5.6}$$

where

$$\begin{aligned} D_c &= diag\{\alpha_1\beta_1, \alpha_2\beta_2, \alpha_3\beta_3\}, \\ D_\sigma &= diag\{\alpha_{\sigma_1}\beta_{\sigma_1}, \alpha_{\sigma_2}\beta_{\sigma_2}, \alpha_{\sigma_3}\beta_{\sigma_3}\}. \end{aligned} \tag{5.7}$$

According to Lyapunov's indirect method, the system is locally asymptotically stable in ζ_* if the eigenvalues of A all have negative real parts. For a constant M, R_c, and K_c, this is found to be the case when $\alpha_i\beta_i >> \alpha_{\sigma_i}\beta_{\sigma_i}$ for $i = 1, 2, 3$.

We select

$$\begin{aligned} \alpha &= (7.5, 1.4, 1.4)^\top \\ \beta &= (150, 40, 30)^\top \\ \alpha_\sigma &= (9.25, 1.7, 2.2)^\top \\ \beta\sigma &= (4.5, 1.0, 1.5)^\top \\ K_c &= diag\{0.2, 0.2, 0.2\} \\ R_c &= diag\{0.0005, 0.001, 0.001\}. \end{aligned} \tag{5.8}$$

The experimental results of this control are shown in Figure 5.5.

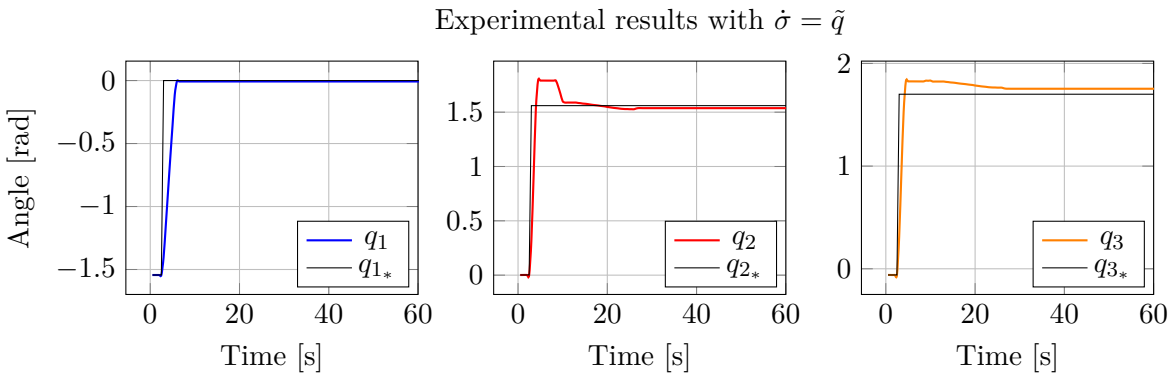

Figure 5.5: Experimental results of the saturated controller with integral term

The steady-state error is eliminated. However, the convergence is very slow and an overshoot is introduced in q_2 and q_3. The difference in performance between the different angles might be due to the fact that q_1 is controlled directly and q_2 and q_3 are controlled by a differential drive. Another factor might be that the motor for q_1 has a higher voltage than the differential drive. Finally, the internal friction of the motor of q_1 is larger than that of the differential drive. This causes more natural damping and can affect the performance.

Next, we modify the dynamics of σ by introducing an additional term. To speed up the convergence of σ, we can adjust the dynamics (5.5) with

$$\dot{\sigma} = \tilde{q} - R_\sigma \sigma, \tag{5.9}$$

with R_σ a diagonal matrix with positive entries. The additional term forces σ to zero faster.

We can linearize the modified system with

$$A_f = \frac{\partial f}{\partial \zeta}\Big|_{\zeta_*} = \begin{bmatrix} 0_{3\times3} & M^{-1} & 0_{3\times3} & 0_{3\times3} \\ -D_c & 0_{3\times3} & -D_c & -D_\sigma \\ -R_cD_c & 0_{3\times3} & -R_cK_c - R_cD_c & 0_{3\times3} \\ I_{3\times3} & 0_{3\times3} & 0_{3\times3} & -R_\sigma \end{bmatrix}. \tag{5.10}$$

Again, ζ_* is an asymptotically stable equilibrium of the closed-loop system if the eigenvalues of A all have negative real parts. This is again the case, if all other gains are constant, when $\alpha_i\beta_i >> \alpha_{\sigma_i}\beta_{\sigma_i}$ for $i = 1, 2, 3$. We select

$$\begin{aligned} \alpha &= (7.5, 1.4, 1.4)^\top \\ \beta &= (150, 40, 30)^\top \\ \alpha_\sigma &= (9.25, 1.7, 2.2)^\top \\ \beta\sigma &= (4.5, 1.0, 1.5)^\top \\ K_c &= diag\{0.2, 0.2, 0.2\} \\ R_c &= diag\{0.0005, 0.001, 0.001\} \\ R_\sigma &= diag\{0.1, 0.12, 0.1\}. \end{aligned} \tag{5.11}$$

The experimental results are shown in Figure 5.6.

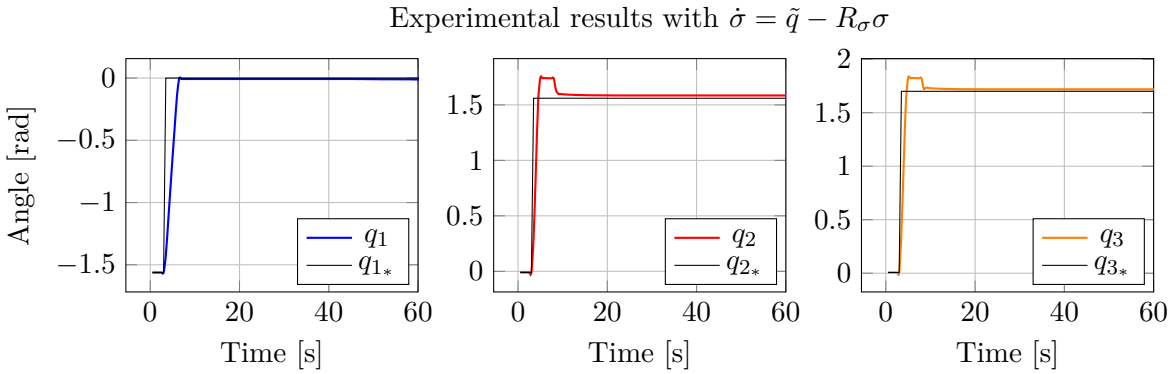

Figure 5.6: Experimental results of the saturated controller with integral term $\dot{\sigma} = \tilde{q} - R_\sigma\sigma$

This figure shows a better performance than Figure 5.5. As expected, the angles converge faster towards their desired positions. Additionally, the overshoot of q_2 and q_3 is smaller. However, the convergence slows down when the error becomes very small.

Next, we introduce the third modification of the dynamics of σ. To speed up the convergence when the angles are close to the desired position, we can adjust the system with

$$\dot{\sigma} = \frac{\partial^2 \Psi}{\partial \sigma^2} \tilde{q}. \tag{5.12}$$

The Hessian of Ψ is a diagonal matrix with entries $\alpha_{\sigma_i} \beta_{\sigma_i} \operatorname{sech}(\beta_{\sigma_i} \sigma_i)$, for $i = 1, 2, 3$. These hyperbolic secants are zero, except for when their arguments are close to zero, with the highest point at zero. Therefore, the value of σ changes more rapidly when it is close to zero. We can linearize the system with

$$A_f = \frac{\partial f}{\partial \zeta}\Big|_{\zeta_*} = \begin{bmatrix} 0_{3\times3} & M^{-1} & 0_{3\times3} & 0_{3\times3} \\ -D_c & 0_{3\times3} & -D_c & -D_\sigma \\ -R_c D_c & 0_{3\times3} & -R_c K_c - R_c D_c & 0_{3\times3} \\ D_\sigma & 0_{3\times3} & 0_{3\times3} & 0_{3\times3} \end{bmatrix}. \tag{5.13}$$

Similar to previous cases, the eigenvalues of A are found have negative real parts when $\alpha_i \beta_i >> \alpha_{\sigma_i} \beta_{\sigma_i}$ for $i = 1, 2, 3$, if all other gains are constant. We select the parameters as (5.8). The experimental results are shown in Figure 5.7.

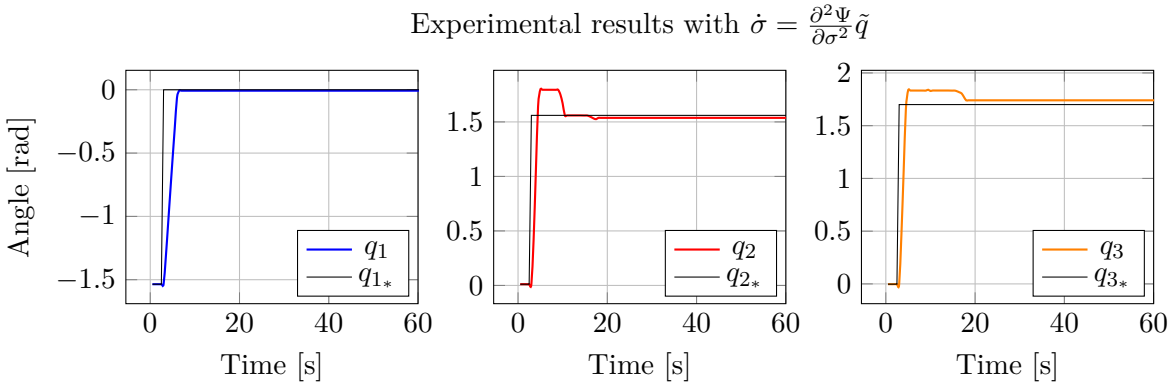

Figure 5.7: Experimental results of the saturated controller with integral term $\dot{\sigma} = \frac{\partial^2 \Psi}{\partial \sigma^2} \tilde{q}$

We see little improvement over the original result in Figure 5.5, in terms of overshoot and convergence. However, we can combine the previously mentioned control methods by defining

$$\dot{\sigma} = \frac{\partial^2 \Psi}{\partial \sigma^2} \tilde{q} - R_\sigma \sigma \tag{5.14}$$

and linearizing the system with

$$A_f = \frac{\partial f}{\partial \zeta}\Big|_{\zeta_*} = \begin{bmatrix} 0_{3\times3} & M^{-1} & 0_{3\times3} & 0_{3\times3} \\ -D_c & 0_{3\times3} & -D_c & -D_\sigma \\ -R_c D_c & 0_{3\times3} & -R_c K_c - R_c D_c & 0_{3\times3} \\ D_\sigma & 0_{3\times3} & 0_{3\times3} & -R_\sigma \end{bmatrix}. \tag{5.15}$$

Again, the eigenvalues of A have negative real parts when $\alpha_i\beta_i >> \alpha_{\sigma_i}\beta_{\sigma_i}$ for $i = 1, 2, 3$, if all other gains are constant. We select the parameters as (5.11). The experimental results of this control law are shown in Figure 5.8.

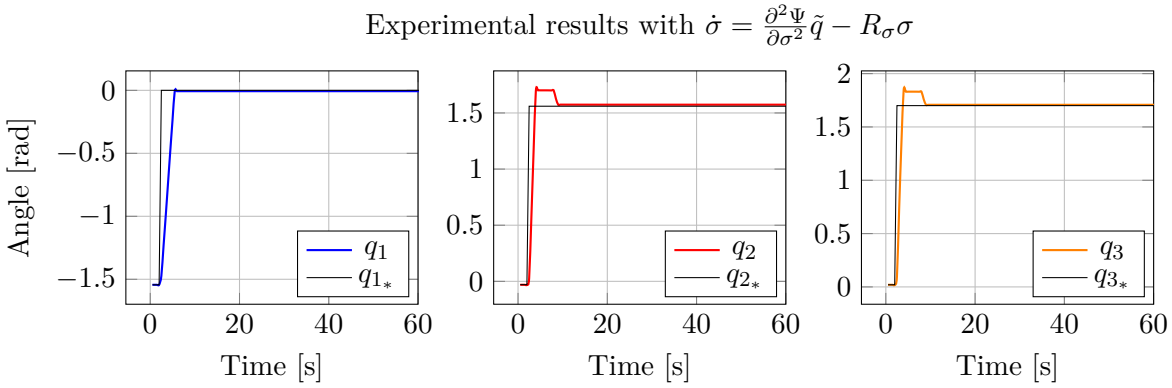

Figure 5.8: Experimental results of the saturated controller with integral term $\dot{\sigma} = \frac{\partial^2\Psi}{\partial\sigma^2}\tilde{q} - R_\sigma\sigma$

We can see a clear improvement over the results of initial integral term in Figure 5.5. The angles converge faster to the desired position and overshoot still is reduced. After the initial overshoot, q_2 and q_3 converge quickly to the desired angles.

It can be concluded that the control law with the best performance of the ones tested in this thesis is given by

$$u = \frac{\partial V}{\partial q} - \frac{\partial \Phi}{\partial z} - \frac{\partial \Psi}{\partial \sigma}, \tag{5.16}$$

with

$$\begin{aligned} \frac{\partial \Phi}{\partial z} &= \sum_{i=1}^{n} e_i \alpha_i \tanh(\beta_i z_i) \\ \frac{\partial \Psi}{\partial \sigma} &= \sum_{i=1}^{n} e_i \alpha_{\sigma_i} \tanh(\beta_{\sigma_i} \sigma_i) \\ \dot{\sigma} &= \frac{\partial^2 \Psi}{\partial \sigma^2}\tilde{q} - R_\sigma \sigma. \end{aligned} \tag{5.17}$$

5.4 Non-saturated control

In this section, the saturated control law is compared against a non-saturated control law to verify its performance. First, to better examine the performance of the saturated control law, a more elaborate depiction of the experimental results is given in Figure 5.9. The first row shows again the real and desired angles over time. In the second row, the motor inputs derived from the control law are given in $[Nm]$. The first graph shows the input for the shoulder yaw motor, u_1. The second graph shows the input for the first motor of the elbow differential drive, $u_2 + u_3$. The third graph shows the input for the second motor of the elbow differential drive, $u_2 - u_3$. The third row of the figure shows the actual motor inputs in $[mA]$. The graphs again show the inputs for the shoulder motor, the first motor of the elbow differential drive and the second motor of the differential drive.

Recall the limits for the motor inputs defined in section 3.8. The second row shows that the motor inputs from the control laws do not exceed the limits. The input to the shoulder yaw motor efficiently approaches the limit of 17.1007. The input to the first motor of the elbow differential drive remains quite small. This is logical as the rotation of this motor is relatively small compared to the second motor. This can be seen in the third graph, as it quickly approaches the limit of 7.901. The third row shows that the actual input to the motors has the same form as the input from the control laws and that the limits in $[mA]$ are never exceeded either.

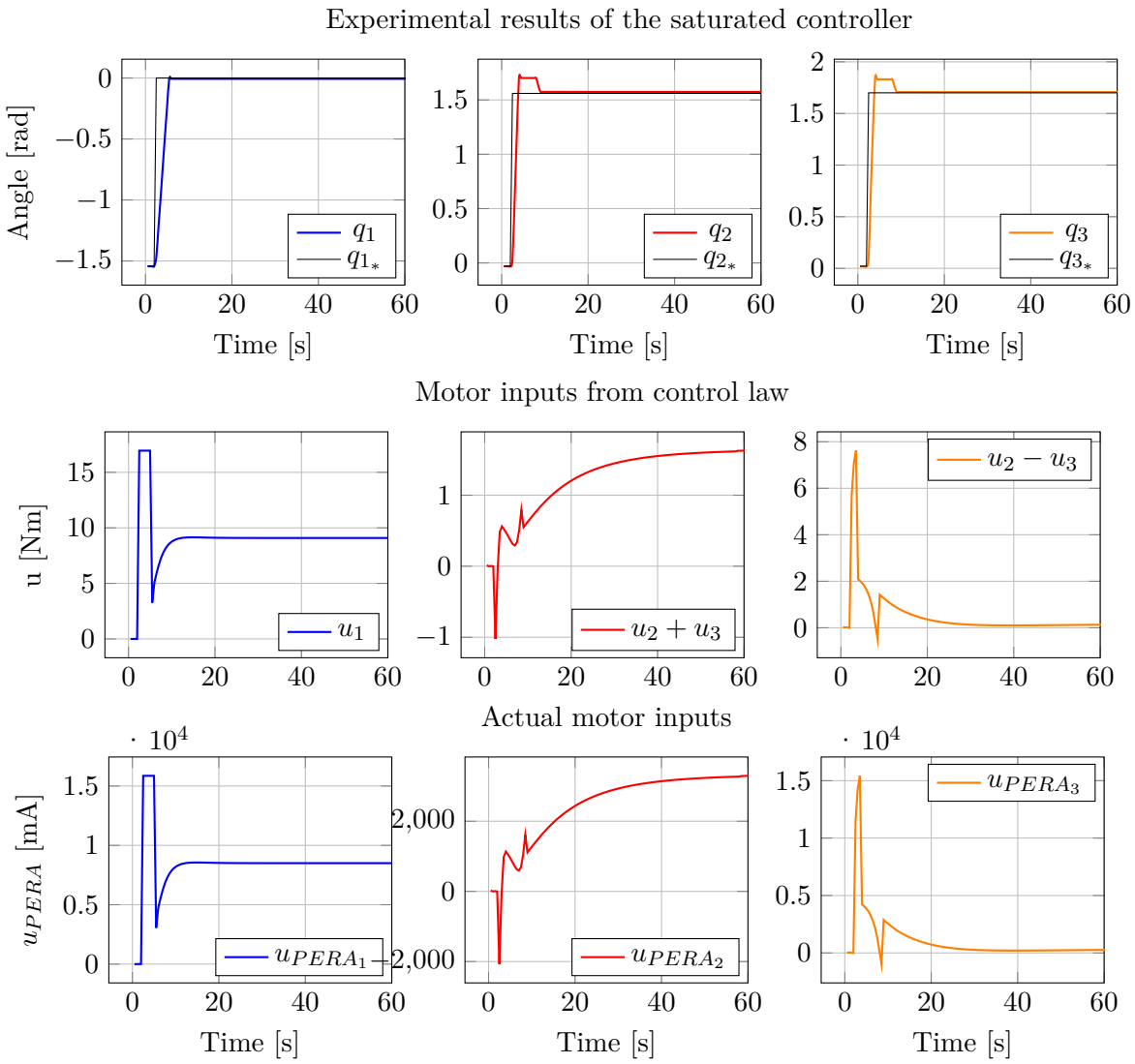

Figure 5.9: Experimental results of the saturated controller

Next, the non-saturated control law is defined as

$$u := \frac{\partial V}{\partial q} - \frac{\partial \Phi}{\partial z} - \frac{\partial \Psi}{\partial \sigma}, \tag{5.18}$$

with

$$\begin{aligned} \frac{\partial \Phi}{\partial z} &= \sum_{i=1}^{n} e_i \alpha_i z_i \\ \frac{\partial \Psi}{\partial \sigma} &= \sum_{i=1}^{n} e_i \alpha_{p_i} \sigma_i \\ \dot{\sigma} &= \Gamma \tilde{q} - R_\sigma \sigma \\ \Gamma &= \sum_{i=1}^{n} e_i e_i^\top \alpha_{p_i} \operatorname{sech}(\beta_{p_i} \sigma_i). \end{aligned} \tag{5.19}$$

Here, z_i is defined as in (4.49). This control law is chosen to closely resemble the form of saturated control law. The results of the experiment are shown in Figure 5.11.

From the first row, it can be concluded that the non-saturated control law performs worse than the saturated version. Compared to Figure 5.9, an overshoot is introduced for q_1, the overshoot in q_2 is increased and the convergence of q_3 to q_{3_*} takes slightly longer. This can be explained by the fact that the second and third term of (5.18) decrease faster than the saturated control law, when q is close to q_*. The saturated control law benefits from its hyperbolic tangents, as these ensure that a constant signal can be generated until q is very close to q_*, as long as β is significantly large. This is illustrated in Figure 5.10.

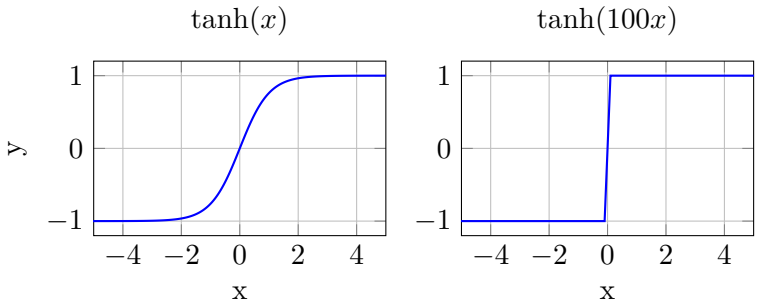

Figure 5.10: Plots of $y = \tanh(\beta x)$, with $\beta = 1$ and $\beta = 100$

Because of this reason, the non-saturated control law relies more on the integral term when q is close to q_*. This causes a larger overshoot to occur.

The second row of Figure 5.11 shows that the motor inputs from the control law for the

shoulder motor and the second motor of the elbow differential drive do not stay within the limits defined in section 3.8. This is the reason that the shapes of the graphs of the second and third row are not the same, as the additional fail-safe cuts of the actual motor inputs at the limit of 16000$[mA]$.

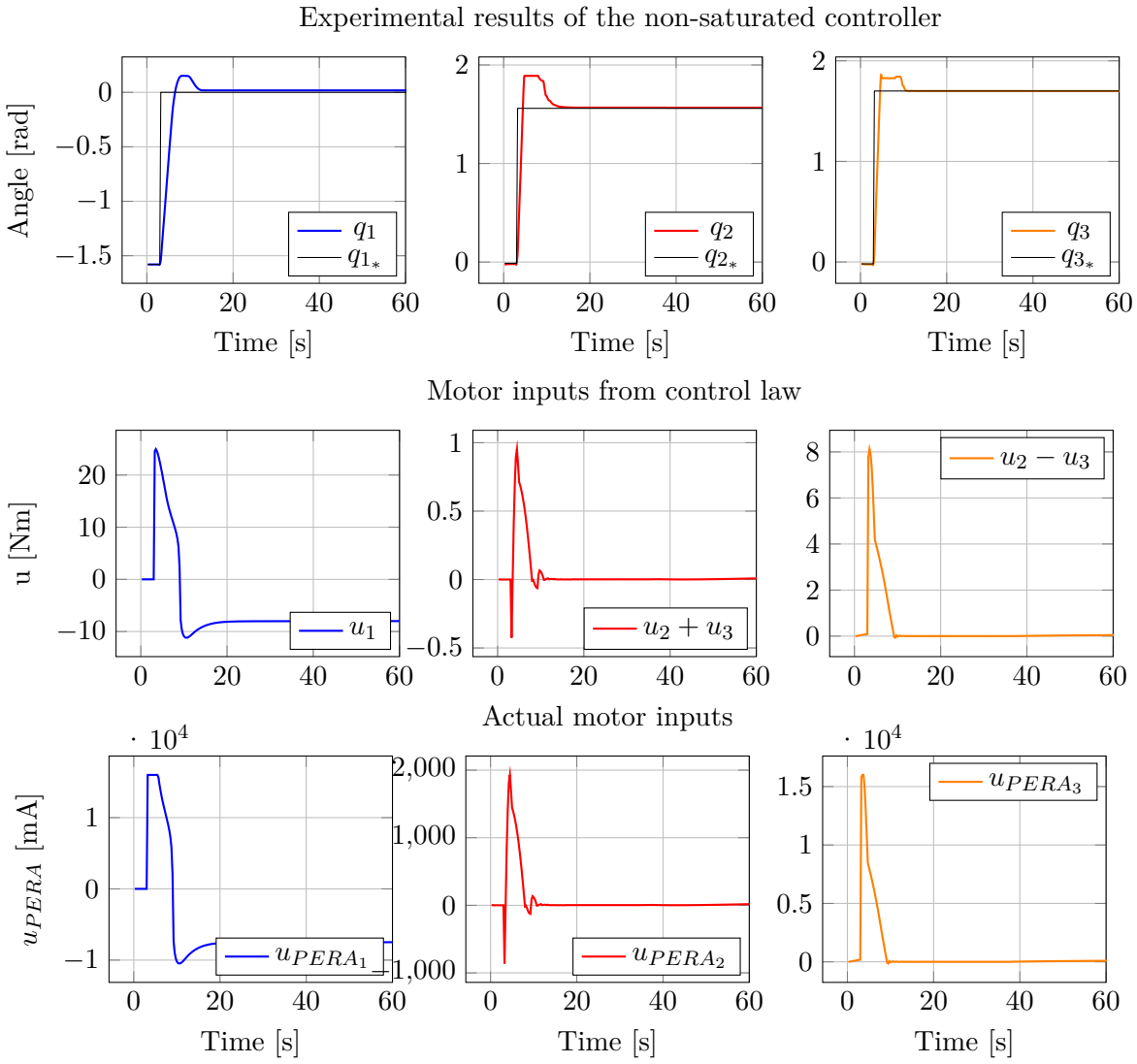

Figure 5.11: Experimental results of the non-saturated controller

5.5 Gripper control

In this section, the gripper control strategy, introduced in section 4.4, is tested. In the experiment, a plastic bottle filled with dried chickpeas is poured empty.

Before implementing the control strategy, the internal force must be approximated. To do this, we measure the force readings while opening and closing the gripper five times. The results of these measurements are shown in Figure 5.12, represented by the colored marks. The internal force due to the spring is observed between 0 and 0.25 radians. After this, the spring is in its rest position. However, some internal force arises between approximately 0.35 and 0.75 radians. The cause for this force should be further investigated.

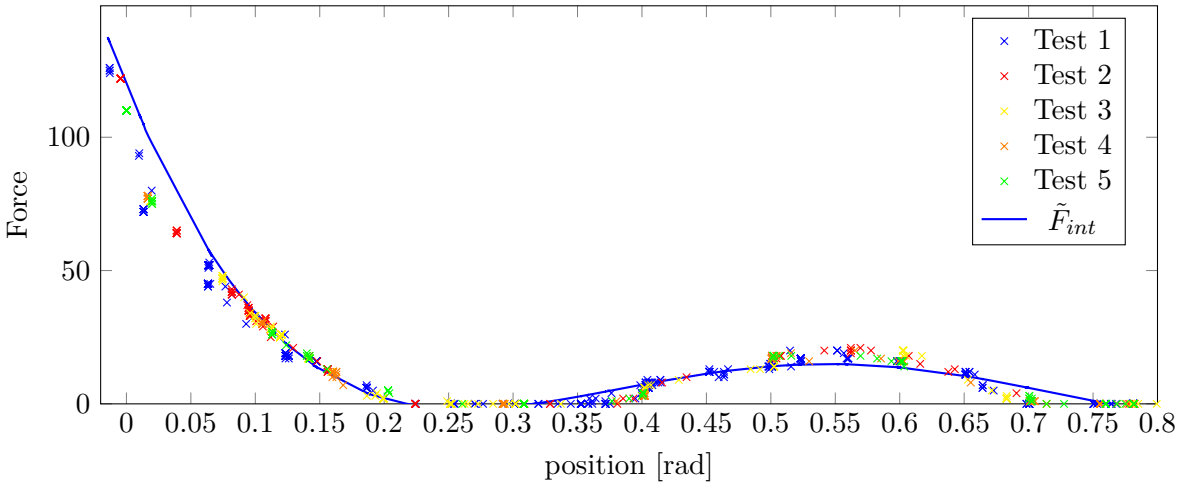

Figure 5.12: Measurements of internal force of the gripper

To approximate the internal force, a fourth degree polynomial trendline is fitted to the data. Using Microsoft Excel, the following approximation of the internal force is found

$$\tilde{F}_{int} = 2564.4q_4^4 - 5629.6q_4^3 + 4206.6q_4^2 - 1229.2q_4 + 120.45. \tag{5.20}$$

This approximated internal force is represented in Figure 5.12 by the blue line. The force measurements used in the control strategy are subtracted by this approximation.

Now, we can start implementing the control strategy. First, the saturated control law (5.16)-(5.17) is implemented in the gripper. During this implementation, we assume the partial derivative of the potential energy to be zero. In reality, this is not the case due to the

spring. However, the form of this potential energy is not precisely known and its magnitude is relatively small. Next, the moving-average filter and control sequence as defined in section 4.4 are implemented, with $m = 50$, $l = 20$. The initial desired position for the 3 DOF PERA is set to $q_* = (-1.56, 1.56, 0)$, with q_{4_*} slightly smaller than the exterior of the bottle to exert enough force to hold the bottle. Figure 5.13 shows this initial position.

Figure 5.13: Start position

Figure 5.14: Final position

Then, the desired position for the elbow yaw is changed to $q_{3_*} = 1.8$, such that the bottle is poured empty (Figure 5.14). The resulting graphs of the positions and forces are shown in Figure 5.15. In the upper graph, the angle of the gripper is shown with its desired angle. The angle of the elbow yaw is shown to indicate when the pouring starts. The lower graph shows the measured force and the moving-average filtered force.

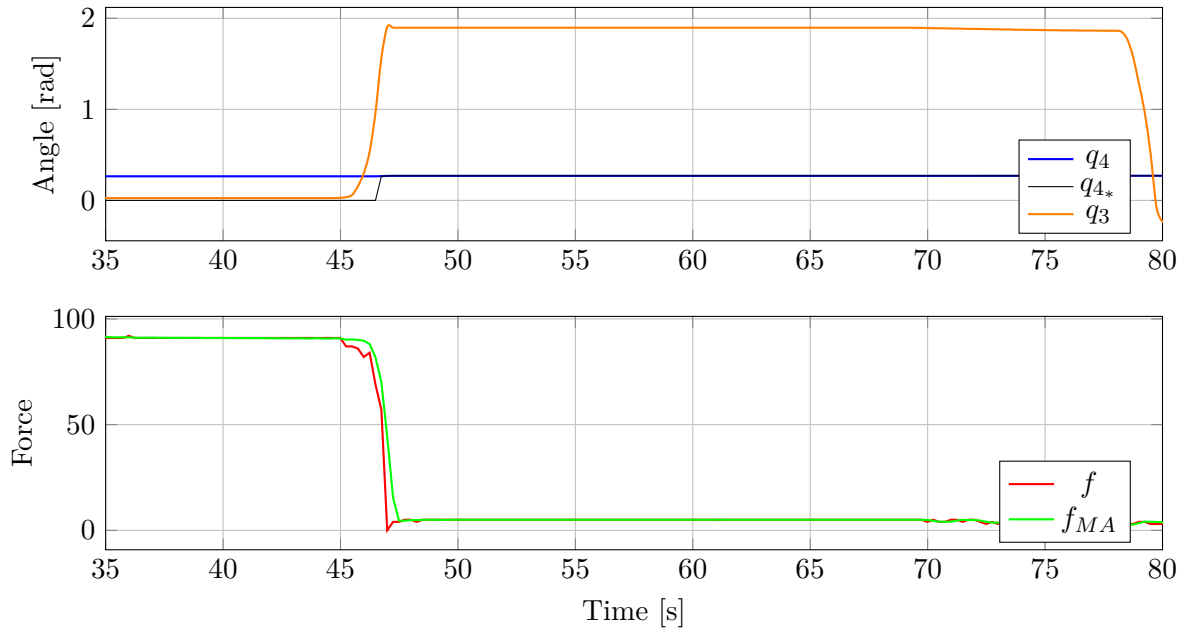

Figure 5.15: Experimental results

The experiment starts at 35 seconds. This is because before that time, the experiment is set up. In the initial position, the desired position of the gripper is smaller than the actual position. This is due to the normal force of the filled bottle, which can be seen in the lower graph. At 45 seconds, the desired position for the elbow yaw is changed and the pouring starts. The measured force rapidly declines as the content of the bottle is poured out and the control sequence responds at 47 seconds by setting the desired position of the gripper equal to the actual position.

We can conclude that the designed control sequence works. It responds when the external force drops away. At 47 seconds, the average measured forces are significantly lower than the average forces measured before that time. The desired position of the gripper is than changed to the current position to prevent it from further pressing in the bottle. However, there are certain drawbacks to this control strategy. The parameters for l and m depend strongly on the pouring vessel, i.e. the bottle, and the pouring substance, i.e. the chickpeas, limiting the robustness of the control. Another drawback is the fact that this control strategy is performed in combination with the control law that regulates the gripper position. A more elegant solution would be to incorporate force feedback into the control law. These issues can be investigated in future research.

Chapter 6

Conclusion

This thesis provides a pouring application for the PERA, whereby the desired gripper position is controlled by the measured force caused by the gripped object. To achieve set point regulation for the gripping application, a control law is designed that is fully saturated and does not require velocity measurements. In contrast to [24] and [25], this control law includes gravity compensation, such that it can be applied to systems with vertical movement. While the omission of velocity measurements is based on [4], the control strategy used in this thesis does not require the solving of partial differential equations.

During the experiments with the 3 DOF PERA, it is concluded that the designed control law achieves the desired positions with a small steady-state error. To compensate for this an integral term is introduced. Multiple integral strategies are compared against each other to find the optimal one. The inclusion of this integral term eliminates the steady-state error quickly, but introduces a small overshoot. For future applications, it should be considered whether a small steady-state error or an overshoot are less desirable.

The designed control law including the integral term is compared against a non-saturated control law to verify the performance. It is concluded that the saturated control law performs better in terms of overshoot and convergence time and that the non-saturated control law indeed leads to motor inputs that exceeds the limits of the motor.

6.1 Future research

Several issues can be addressed in future research. During the thesis, certain assumptions are made that can be further investigated. The first one being the natural damping of the system. During the experiments, it is noticed that the joints of the PERA have significant friction. However, this is not taken into account in the design of the control law or in the simulations. Future research can approximate this damping and incorporate this in the control law.

Another issue for future research is the application of variable gains. In the experiments performed during this thesis, all gains are set at a constant value. However, it might be more efficient to introduce gains, which are variable and respond to the desired positions.

A third issue is the port-Hamiltonian structure. After implementing the integral term, the port-Hamiltonian structure of the closed-loop system is lost. Therefore, the asymptotic stability of the equilibria can not as easily be concluded. An opportunity for future research is to find an integral term which can be incorporated in the Hamiltonian structure.

As mentioned before, the control sequence for the gripper has some drawbacks. The robustness can be further increased as it now depends heavily on the pouring vessel and the pouring substance. Furthermore, the force feedback can be incorporated into the control law.

Finally, additional applications can be created with the designed control law. A simple first step is to integrate more DOFs of the PERA in an application. However, other applications, such as trajectory tracking can be pursued, visual input can be included or other applications for the gripper can be created.

Appendices

Appendix A

PERA Wiring Diagram

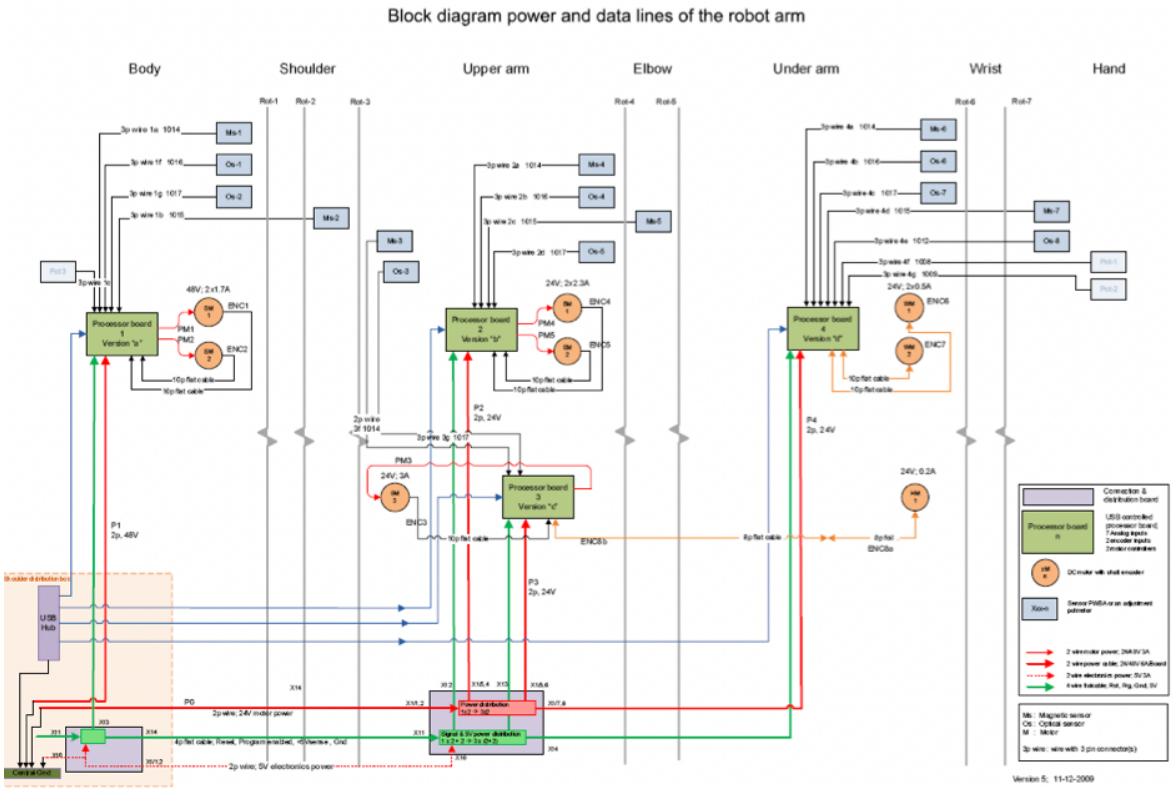

Appendix B

Wiring Changes PERA

Some changes were made to the wiring of the PERA. Specifically, the force sensory of the gripper is connected to Board 4 (Wrist), instead of Board 3 (Shoulder/Gripper). The wires, marked with label 12, are connected to input port 1012 on the board, corresponding to signal $ADC2$. For more information on the boards, see [19].

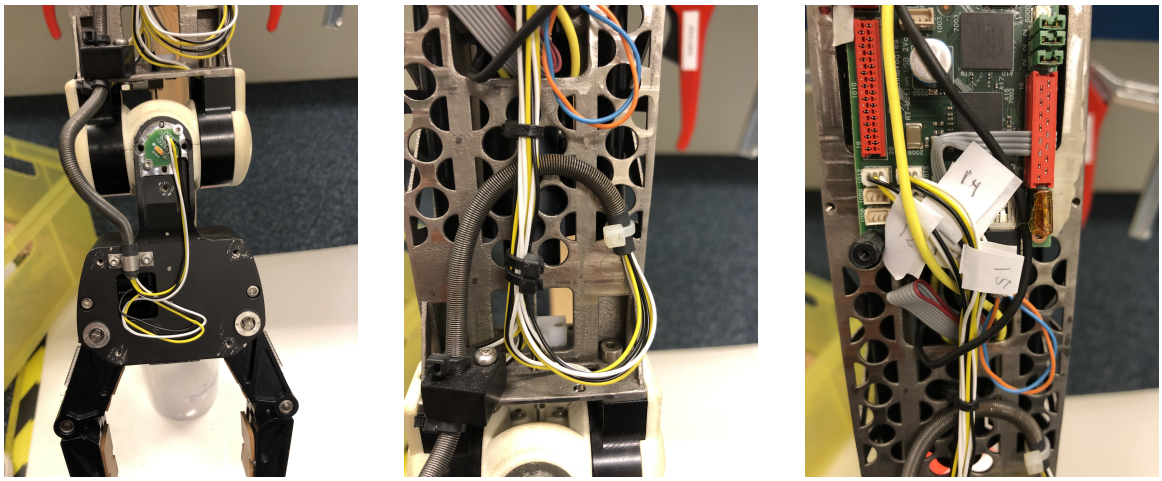

Figure B.1: Wiring of gripper sensors

References

[1] M. Bol, "Force and position control of the philips experimental robot arm in an energy based setting," Master's thesis, University of Groningen, 2012.

[2] P. Borja, R. Cisneros, and R. Ortega, "A constructive procedure for energy shaping of port—hamiltonian systems," *Automatica*, vol. 72, pp. 230–234, 2016.

[3] J. J. Craig, *Introduction to Robotics*. Pearson, 2005.

[4] D. A. Dirksz, J. M. Scherpen, and R. Ortega, "Interconnection and damping assignment passivity-based control for port-hamiltonian mechanical systems with only position measurements," in *2008 47th IEEE Conference on Decision and Control*. IEEE, 2008, pp. 4957–4962.

[5] V. Duindam, A. Macchelli, S. Stramigioli, and H. Bruyninckx, *Modeling and control of complex physical systems: the port-Hamiltonian approach*. Springer Science & Business Media, 2009.

[6] A. Flores-Abad, O. Ma, K. Pham, and S. Ulrich, "A review of space robotics technologies for on-orbit servicing," *Progress in Aerospace Sciences*, vol. 68, pp. 1–26, 2014.

[7] M. Hägele, K. Nilsson, and J. N. Pires, "Industrial robotics," *Springer handbook of robotics*, pp. 963–986, 2008.

[8] D. Hill and P. Moylan, "The stability of nonlinear dissipative systems," *IEEE Transactions on Automatic Control*, vol. 21, no. 5, pp. 708–711, 1976.

[9] R. Kelly, V. S. Davila, and J. A. L. Perez, *Control of robot manipulators in joint space*. Springer Science & Business Media, 2006.

[10] H. K. Khalil, *Nonlinear Systems*. Prentice-Hall, 1996.

[11] F. Koops, "Trajectory tracking control of the philips experimental robot arm in the port-hamiltonian framework," Master's thesis, University of Groningen, 2014.

[12] B. M. Maschke and A. J. van der Schaft, "Port-controlled hamiltonian systems: modelling origins and systemtheoretic properties," *IFAC Proceedings Volumes*, vol. 25, no. 13, pp. 359–365, 1992.

[13] P. Moylan, "Dissipative systems and stability," *Lecture Notes in collaboration with D. Hill, University of Newcastle, www. pmoylan. org*, 2014.

[14] M. Muñoz-Arias, "Energy-based control design for mechanical systems: Applications of the port-hamiltonian approach," Ph.D. dissertation, University of Groningen, 2015.

[15] R. Ortega and E. Garcia-Canseco, "Interconnection and damping assignment passivity-based control: A survey," *European Journal of control*, vol. 10, no. 5, pp. 432–450, 2004.

[16] R. Ortega, J. A. L. Perez, P. J. Nicklasson, and H. J. Sira-Ramirez, *Passivity-based control of Euler-Lagrange systems: mechanical, electrical and electromechanical applications*. Springer Science & Business Media, 2013.

[17] R. Ortega and M. W. Spong, "Adaptive motion control of rigid robots: A tutorial," *Automatica*, vol. 25, no. 6, pp. 877–888, 1989.

[18] R. Ortega, A. J. Van Der Schaft, I. Mareels, and B. Maschke, "Putting energy back in control," *IEEE Control Systems Magazine*, vol. 21, no. 2, pp. 18–33, 2001.

[19] R. Rijs, R. Beekmans, S. Izmit, and D. Bemelmans, "Philips experimental robot arm, user instruction manual v1.1," 2010.

[20] J. Siemonsma, "Design and implementation of a nonlinear force controller for the philips experimental robot arm," Bachelor's thesis, University of Groningen, 2014.

[21] M. W. Spong, S. Hutchinson, and M. Vidyasagar, *Robot Dynamics and Control*. Wiley, 2004.

[22] M. Takegaki and S. Arimoto, "A new feedback method for dynamic control of manipulators," *Journal of Dynamic Systems, Measurement, and Control*, vol. 103, no. 2, pp. 119–125, 1981.

[23] A. J. van der Schaft, *L2-gain and passivity techniques in nonlinear control*. Springer, 2000, vol. 2.

[24] A. Veltman, "Pick and place routines with a flexible joint robotic arm using passivity-based control," Master's thesis, University of Groningen, 2019.

[25] T. Wesselink, P. Borja, and J. M. Scherpen, "Saturated control without velocity measurements for planar robots with flexible joints," in *58th IEEE Conference on Decision and Control*. IEEE, 2019, to appear.

[26] J. C. Willems, "Dissipative dynamical systems part i: General theory," *Archive for rational mechanics and analysis*, vol. 45, no. 5, pp. 321–351, 1972.